Title	Studies on Photoinduced Reaction Systems for Carbon Dioxide Fixation
Author(s)	井上, 博史
Citation	大阪大学, 1995, 博士論文
Version Type	VoR
URL	https://doi.org/10.11501/3104981
rights	
Note	

Studies on
Photoinduced Reaction Systems for
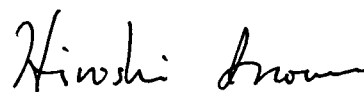# Carbon Dioxide Fixation

（二酸化炭素固定のための光誘起反応システムに関する研究）

1995

Hiroshi Inoue

Department of Applied Chemistry
Faculty of Engineering
Osaka University

Preface

The work of this thesis was carried out under the guidance of Professor Dr. Hiroshi Yoneyama at Department of Applied Chemistry, Faculty of Engineering, Osaka University for six years since 1989.

The objective of this thesis is the establishment of photo-induced reaction systems for carbon dioxide fixation. The author hopes that the findings obtained in this work afford some suggestions for the development of the effective usage of carbon dioxide.

Hiroshi Inoue

Department of Applied Chemistry,
Faculty of Engineering,
Osaka University,
Yamada-oka 2-1, Suita, Osaka 565, Japan
March / 1995

Contents

General Introduction

The photoreductions and photochemical fixations of CO_2 molecules under mild conditions have attracted intensive attention from the viewpoint of not only the production of industrially useful compounds but also of the conversion and storage of solar energy to chemical energy. Investigations on various homogeneous and heterogeneous photoreductions[1-18] of CO_2 molecules and photochemical fixations[1,19-28] of CO_2 in organic molecules to produce industrially useful compounds have been actively performed. As a result, a variety of photo-induced reduction and fixation systems have been investigated using semiconductor photocatalysts such as TiO_2,[2-10] GaP,[2] SiC,[11,12] CdS,[2,3,13a,14,15] Ni_2S_3,[14] Si,[16] ZnS,[13b,17] and Cu_2O,[18] metal complex photocatalysts such as metalloporphyrins,[19] metal tetraazamacrocycles,[20] and metal bipyridine,[21-24] and organic compound photosensitizers such as pyrene,[25] oligo(p-phenylene),[26] poly(p-phenylene)[27] and poly(pyridine-2,5-diyl).[28] However, since these photo-induced reaction systems do not give high photoconversion efficiency except for works done by Henglein et al.,[17] where a 80 % of quantum efficiency for photoreduction of CO_2 to formate was reported with use of ZnS microcrystals as the photocatalyst, the search of new systems and/or the development of active photocatalysts are desired. In this study, the following two approaches were investigated to develop efficient photo-induced reduction and fixation systems of CO_2.

(1) Development of photochemical CO_2 fixation processes from electrochemical CO_2 fixation systems with high current efficiencies.

Isocitrate dehydrogenase and malic enzyme catalyze in vivo the oxidative decarboxylation of isocitrate and malate to give oxoglutarate and pyruvate, respectively. It was already reported that the reverse to these spontaneous

1

reactions occurs by electrochemical means with ca. 100% of current efficiency at such low overvoltage[29] as not achieved in the other electrochemical CO_2 reduction and fixation systems without use of the enzyme. In this study, photo-induced reactions of these electrochemical enzymatic CO_2 fixations were investigated using semiconductor particles as photocatalysts.

(2) Photoreduction of CO_2 using semiconductor microcrystalline photocatalysts.

Semiconductor microcrystals having the size quantization effect increase their bandgaps in comparison with the bulk semiconductors due to the confinement of photogenerated electrons and holes in the microcrystals.[30-32] Potentials of the conduction band and the valence band of the semiconductor microcrystals shift to the negative and positive directions, respectively, depending on the degree of the size quantization, resulting in the increase of the oxidation and reduction powers as the photocatalysts.[33] In this regard, it is important to elucidate the effect of particle size of the semiconductor microcrystals on the photocatalytic activity. Besides the enhancement due to the size quantization of the photocatalytic activities, loading of electrocatalysts on the semiconductor surfaces has been employed as a means of enhancing the photocatalytic activities of semiconductor particles for a variety of light-induced heterogeneous reactions. In the present study, therefore, the effect of metal-loading of the semiconductor microcrystal surfaces on the quantum efficiency for photoreduction of CO_2 was also investigated.

Since the semiconductor microcrystals have a general tendency to be coagulated, stabilizers have been used in the preparation of the semiconductor microcrystals to avoid the coagulation. However, the effect of the stabilizers on semiconductor photocatalysis has not been investigated in detail. To clarify the role of stabilizers, the effect of the stabilizers on the photoreduction behaviors of CO_2 was investigated for stabilizers having positive, negative and

2

neutral charges. Recent studies have shown that chemical modification of semiconductor microcrystals is effective as a means for stabilizing the microcrystals. If chemically modified microcrystals are used as photocatalysts, electron transfers across the modified layer must influence more or less the photocatalytic activities of the microcrystals. In the present study, effect of alkyl chain length of alkanethiol-modified ZnS microcrystal on kinetics of the photo-induced electron transfer reaction was studied.

This thesis is composed of the following four chapters.

Chapter 1 describes the photochemical fixation of CO_2 in oxoglutarate and pyruvate using either isocitrate dehydrogenase or malic enzyme and semiconductor photocatalysts. Also described is the photochemical conversion of lactate to malate through pyruvate in the presence of malic enzyme and CdS. Chapter 2 describes the effect of particle size of ZnS and TiO_2 microcrystals on photocatalytic activities for CO_2 reduction. In chapter 3, the effect of metal-loading for ZnS microcrystals on photocatalytic activity for CO_2 reduction and the effect of charged conditions of stabilizers for CdS microcrystals on photoreduction of CO_2 will be described. Chapter 4 describes the preparation of the surface modification of ZnS microcrystals by various alkanethiols and the effect of the modified layer on the photo-induced electron transfer to methyl viologen.

List of publications

1. Effects of Size Quantization of Zinc Sulfide Microcrystallites on Photocatalytic Reduction of Carbon Dioxide

   Inoue, H.; Torimoto, T.; Sakata, T.; Mori, H.; Yoneyama, H.

   Chem. Lett. **1990**, 1483.

2. Photocatalytic Fixation of Carbon Dioxide in Oxoglutaric Acid Using Isocitrate Dehydrogenase and Cadmium Sulphide

   Inoue, H.; Kubo, Y.; Yoneyama, H.

   J. Chem. Soc., Faraday Trans. **1991**, 87, 553.

3. Photocatalytic Conversion of Lactic Acid to Malic Acid through Pyruvic Acid in the Presence of Malic Enzyme and Semiconductor Photocatalysts

   Inoue, H.; Yamachika, M.; Yoneyama, H.

   J. Chem. Soc., Faraday Trans. **1992**, 88, 2215.

4. Photocatalytic Activities for Carbon Dioxide Reduction of TiO_2 Microcrystals Prepared in SiO_2 Matrices Using a Sol-Gel Method

   Inoue, H.; Matsuyama, T.; Liu B. -J.; Sakata, T.; Mori, H.;

   Yoneyama, H.

   Chem. Lett. **1994**, 653.

5. Effect of Charged Conditions of Stabilizers for Cadmium Sulfide Microcrystalline Photocatalysts on Photoreduction of Carbon Dioxide

   Inoue, H.; Nakamura, R.; Yoneyama, H.

   Chem. Lett. **1994**, 1227.

6. Photoinduced Electron Transfer from Zinc Sulfide Microcrystals
   Modified with Various Alkanethiols to Methyl Viologen
   Inoue, H.; Ichiroku, N.; Torimoto, T.; Sakata, T.; Mori, H.;
   Yoneyama, H.
   Langmuir **1994**, 10, 4517.

7. Photoreduction of Carbon Dioxide Using Chalcogenide Semiconductor
   Microcrystals
   Inoue, H.; Moriwaki, H.; Maeda, K.; Yoneyama, H.
   J. Photochem. Photobiol. A: Chem. in press.

Chapter 1 Photochemical Fixation of Carbon Dioxide in Organic Compounds Using Enzymes and Semiconductor Photocatalysts

1-1 Introduction

Recently fairly intensive attention has been paid to the electrochemical[29,34-39] and photochemical[13,19,24,40,41] fixation of CO_2 in a variety of organic molecules under mild conditions. It is well-known[42] that enzymes are very useful as catalysts in organic synthesis with high selectivities and high yields. Concerning the CO_2 fixation chemistry, it is well-established[43,44] that isocitrate dehydrogenase (ICDH) and malic enzyme (ME) work well as biocatalysts for the fixation of CO_2 in oxoglutarate and pyruvate to yield isocitrate and malate, respectively, with the use of the reduced form of nicotinamide adenine dinucleotido phosphate (NADPH) as a sacrificial reagent. Whitesides et al.[45] succeeded in recycling NADPH in this enzymatic CO_2 fixation reaction using electron mediators such as flavin and methyl viologen (MV^{2+}). Willner et al.[24] succeeded in the photochemical fixation of CO_2 in oxoglutarate and pyruvate with the use of either ICDH or ME and MV^{2+} in the presence of $NADP^+$, ferredoxin-$NADP^+$ reductase (FNR), and a sensitizer such as ruthenium trisbipyridine and metalloporphyrins.

The first electrochemical fixation of CO_2 using enzyme as a catalyst was achieved by Parkinson and Weaver[40] who succeeded in reducing CO_2 to formate at illuminated p-type InP electrodes in the presence of formate dehydrogenase and MV^{2+} as an electron mediator. It has recently been discovered[29a] that electrolysis of CO_2-saturated TRIS buffer containing oxoglutarate, ICDH, and MV^{2+} as an electron mediator yielded isocitrate with a current efficiency approaching 100 % and at a low overvoltage. NADPH

was not needed in that case. In addition, electrochemical fixation of CO_2 in pyruvate using ME was also achieved with the current efficiency approaching 100 %,[29b] but both FNR and NADP$^+$ were essential besides MV^{2+} to fix CO_2 in pyruvate. Based on these electrochemical studies, photochemical fixation of CO_2 in oxoglutarate and pyruvate was attempted using photogenerated electrons in semiconductor photocatalysts. The postulated reaction schemes are shown in Fig. 1. Semiconductor photocatalysts used as the photocatalyst must satisfy such energy requirement that photogenerated electrons can energetically reduce MV^{2+}. CdS macrocrystalline powder and TiO_2 microcrystals fixed in the interlayer spacings of sodium montmorillonite,[46] which is represented as TiO_2/clay, meet such energy requirements and then used in the present study as the photocatalysts. Since irradiation of the semiconductor photocatalysts with light of energy greater than its bandgaps generates positive holes as well as electrons, it is important to design the overall photo-induced reaction system with effective utilization of the photogenerated holes. In this chapter, triethanolamine, 2-mercaptoethanol and lactate were used as a highly reactive hole scavenger in order to investigate how easily the CO_2 fixation in oxoglutarate and pyruvate occurs with consumption of photogenerated electrons. Since the oxidation products of triethanolamine and 2-mercaptoethanol, however, do not have a wide utility, further improvements in the present photo-induced reaction systems seem desired in future.

Harada et al.[47] found that lactate was oxidized to pyruvate with the evolution of H_2 at Pt-loaded semiconductor photocatalysts such as CdS and TiO_2. Since pyruvate is a substrate for CO_2 to be fixed with assistance of ME, a reaction scheme shown in Fig. 2 is devised based on that given in Fig. 1(b).
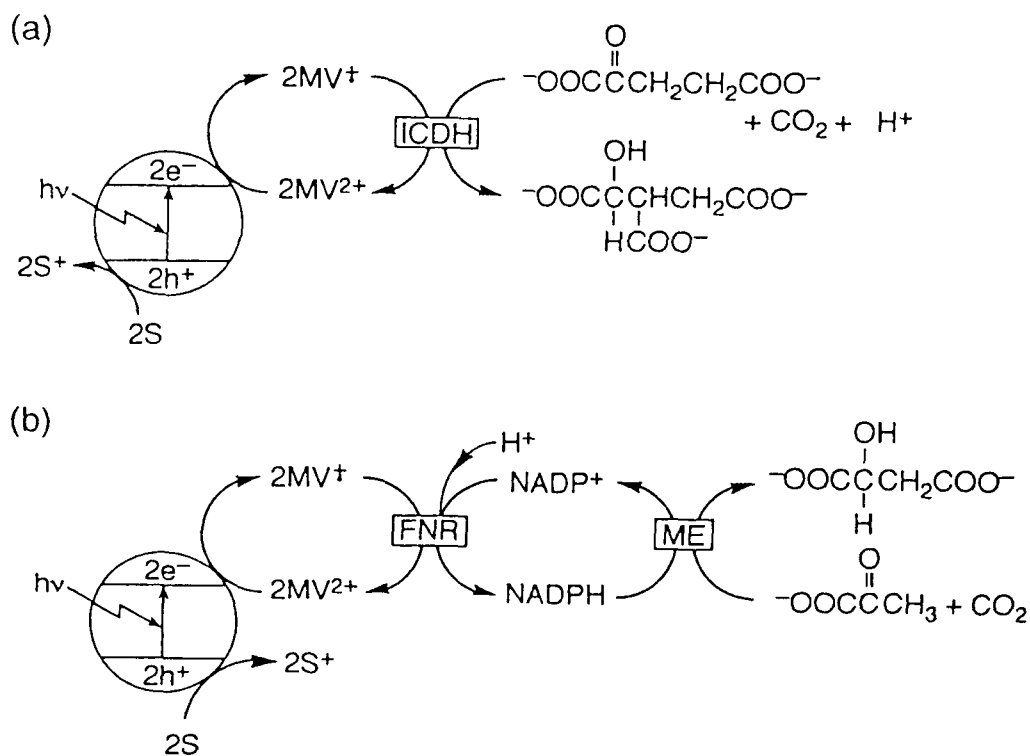
7

Fig. 1. Reaction scheme of the photochemical fixation of CO_2 in (a) oxoglutarate and (b) pyruvate in the presence of either (a) ICDH or (b) ME and semiconductor photocatalysts. S: hole scavenger
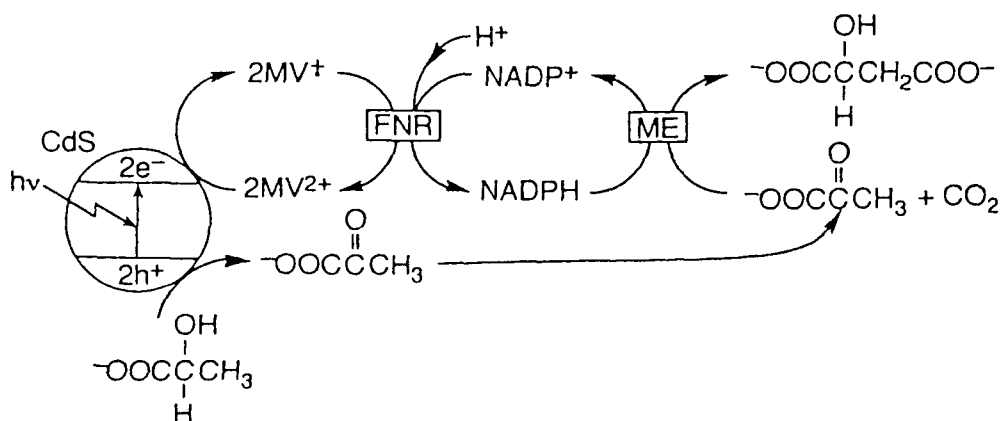

Fig. 2. Reaction scheme of the photochemical conversion of lactate to malate through pyruvate.

1-2 Experimental

Chemicals.

ICDH (from yeast, EC 1.1.1.42), NADP$^+$ and NADPH were used as received from Oriental Yeast. ME (from chicken liver, EC 1.1.1.40) and FNR (from spinach leaves, EC 1.18.1.2) were used as received from Sigma. The other chemicals used in this study were purchased from Wako Pure Chemicals, except for montmorillonite (Nacalai Tesque), methyl viologen (MV^{2+})(Tokyo Kasei) and CdS of 99.99% purity (Mitsuwa). All the chemicals were used without further purification. The measured specific surface area of the CdS powder was 23.1 m^2 g^{-1}. The crystal structure of the CdS powder was wurtzite.

Instruments

TiO$_2$ microcrystals were prepared in the interlayer spacings of sodium montmorillonite. Details of the preparation and characterization of the TiO$_2$/clay were reported in a ref. 46. The specific surface area of the TiO$_2$ microcrystals ranged between 203 and 275 m^{2}g^{-1}. The amount of TiO$_2$ incorporated in the clay was 50 wt%.

Photocatalytic experiments were carried out using Pyrex and quartz cells of ca.160 mm height and 18 mm diameter. For the case of photochemical CO$_2$ fixation in oxoglutarate 4 cm^3 of reaction solution containing 4 mM (mM=mmol dm^{-3}) of suspended CdS was put in the Pyrex cells, while 10 cm^3 of reaction solution containing 1.25 mM of suspended TiO$_2$/clay or CdS was put in the quartz reaction cell for the photochemical CO$_2$ fixation in pyruvate. After the reaction solution was saturated with CO$_2$ gas for 1 h, the cell was closed and illuminated with a 500 W Xe arc lamp (Ushio UI-501C) through a UV-39 cut off filter (Toshiba) when CdS was used as a photocatalyst and with

a 500 W high pressure Hg arc lamp (Ushio UI-501C) through a UV-31 cut off filter (Toshiba) when TiO_2/clay was used. The cell was set in a water bath at 25 °C. The solution was stirred with a magnetic stirrer during illumination.

Changes in the concentration of NADPH caused by the enzymatic and photochemical CO_2 fixations in pyruvate were monitored by absorption spectroscopy at 340 nm (molar absorption coefficient 6200 M^{-1} cm^{-1} [48]) using an HP 8452A diode array spectrophotometer (Hewlett Packard).

Determination of Products

Isocitrate produced in the photocatalytic experiments was determined by using a CCPE high pressure liquid chromatograph (Tosoh) which was equipped with an ODS-80TM column (Tosoh) and a UV-8011 UV detector (Tosoh). The eluent solution was 10 mM $NH_4H_2PO_4$ - 10 mM H_3PO_4 (pH 2.5). The production of malate and pyruvate in the photocatalytic experiments were monitored using a CCPE high-pressure liquid chromatograph equipped with an organic acid column (Waters) and a UV-8011 UV detector (Tosoh). The eluent solution was 0.1% H_3PO_4.

The quantum efficiency for malate production at the TiO_2/clay photocatalysts was determined with illumination of monochromatic light of 313 nm obtained by using a CT-10 monochromater (JASCO). Its full width at half maximum intensity was 6 nm. When the CdS photocatalyst was used the quantum efficiency was determined with illumination at 410 nm obtained by using an interference filter (Vacuum Optics Corporation of Japan). Its full width at half maximum was 14 nm. The quantum efficiency for isocitrate production is defined by the following equation (1).

$$\text{(Quantum efficiency)} = \frac{\text{(Amount of the isocitrate production for 24 h)} \times 2}{\text{(Number of incident photons for 24 h)}} \times 100 \quad (1)$$

The quantum efficiencies for malate production were evaluated in the same way except for the illumination time of 1h. The number of incident photons was determined by ferrioxalate actinometry.

1-3 Results and Discussion

1-3-1 Photochemical Fixation of Carbon Dioxide in Oxoglutarate Using Isocitrate Dehydrogenase and Cadmium Sulfide

The experiments were carried out using 0.2 M TRIS buffer containing 1 mM MV^{2+}, 0.8 unit of ICDH, 1 M triethanolamine, and 0.016 mmol of CdS and oxoglutarate of variable concentration ranging from 1 to 10 mM. The isocitrate production proceeded linearly with the illumination time for the first 8 h, but beyond that the production decreased gradually, resulting in the complete suppression after ca. 20 h (Fig. 3). If 0.8 unit of ICDH was added at this stage, the production of isocitrate began to increase again, suggesting that the decrease in the isocitrate production was at least in part related to the loss of the enzymatic activity.

If it is assumed that 1 unit of ICDH contains 1.5 nmol of the redox centers,[49] the turnover number of ICDH before the loss of activity in the CO_2 fixation system was 6200. The isocitrate production increased with an increase in the initial concentration of oxoglutarate (Fig. 3). If the rate of the isocitrate production as estimated from the slope of the isocitrate production vs. illumination time relations shown in Fig. 3 at an initial stage of illumination was plotted as a function of the concentration of oxoglutarate, Fig. 4 was obtained. In this figure the production rate was dependent on the concentration of oxoglutarate.

Figure 5 shows the time course of the isocitrate production with various
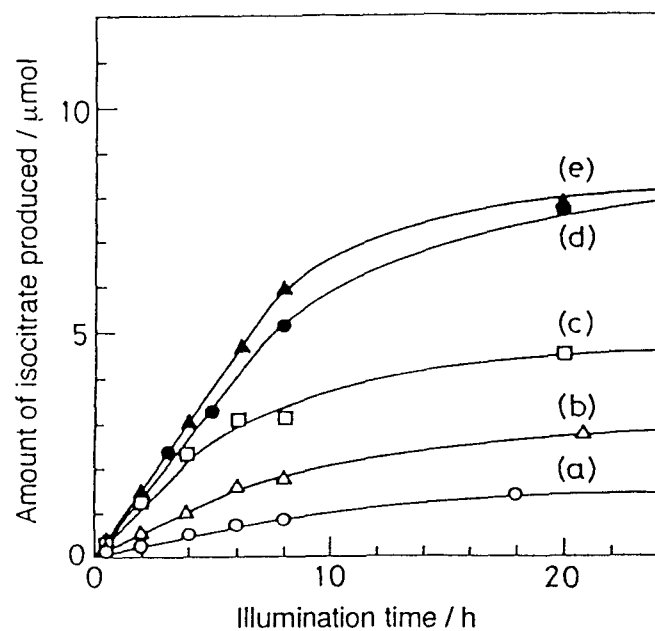
Fig. 3. Time course of production of isocitrate for different concentrations of oxoglutarate: (a) 1 mM, (b) 3 mM, (c) 5 mM, (d) 8 mM, (e) 10 mM. The other solution conditions are shown in the text.
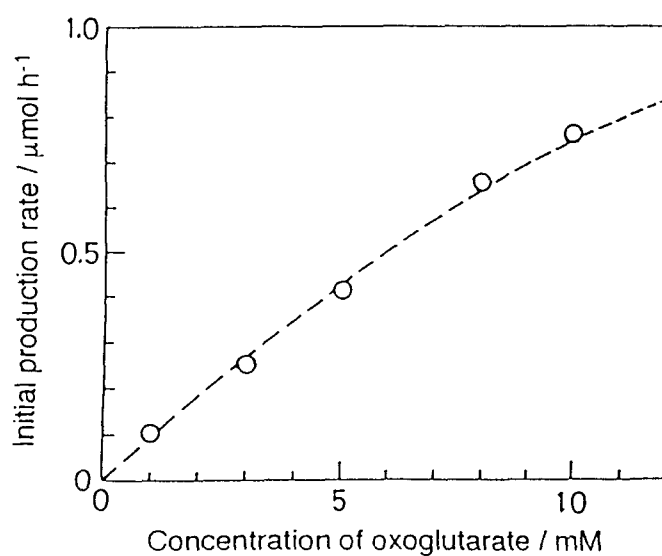

Fig. 4. Initial rate of production of isocitrate as a function of the concentration of oxoglutarate. The dashed curve gives the rate obtained by eq. (16) derived in the text.

12

Fig. 5. Time course of production of isocitrate for different concentrations of MV^{2+}: (a) 0.01 mM, (b) 0.025 mM, (c) 0.25 mM, (d) 1 mM. Concentration of oxoglutarate was 10 mM. The other solution conditions were the same as those given in Fig. 3.

concentrations of MV^{2+} ranging from 0.01 to 1 mM. The solution conditions were the same as those described above except that the concentration of oxoglutarate was 10 mM. In those cases the initial rate of the isocitrate production seemed to increase with increasing the concentration of MV^{2+} up to 0.25 mM, beyond which the rate seemed to become independent of the MV^{2+} concentration as shown in Fig. 6.

Figure 7 shows the effect of the illumination intensity on the time course of isocitrate production obtained with 1 mM MV^{2+}, 10 mM oxoglutarate and 0.8 unit of ICDH. The amount and rate of the isocitrate production increased with increasing the light intensity; if weak light intensities were employed the isocitrate production proceeded linearly with the illumination time even after illumination for 24 h.

The quantum efficiency determined at 410 nm with illumination of

13

Fig. 6. Initial rate of production of isocitrate as a function of the concentration of MV^{2+}. The dashed curve shows the rate obtained by eq. (16) as in the case of Fig. 4.
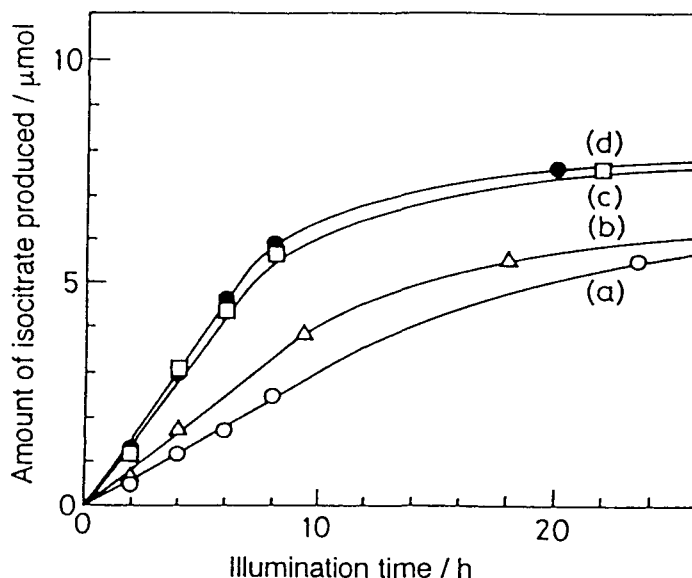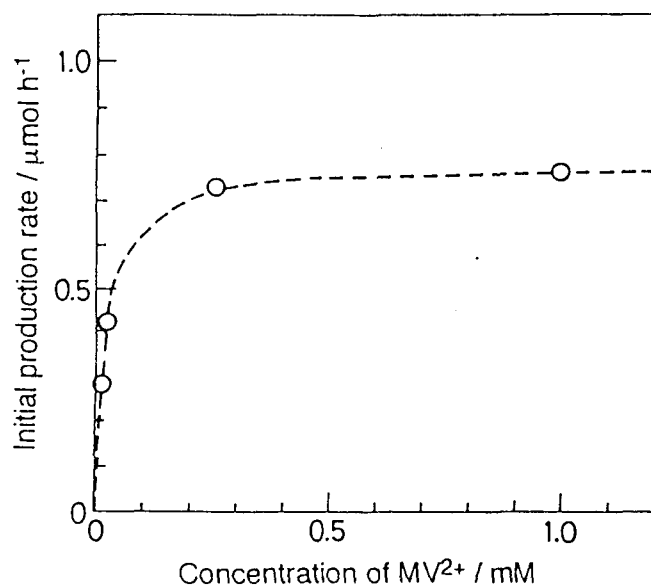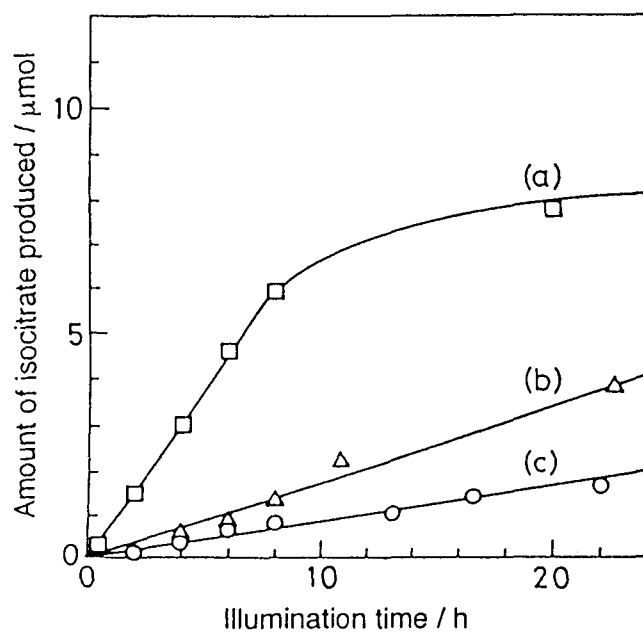

Fig. 7. Time course of production of isocitrate under illumination of different light intensities: (a) 0.53 W cm^{-2}, (b) 0.11 W cm^{-2}, (c) 0.0063 W cm^{-2}. The solution conditions are shown in the text.

0.0013 W cm^{-2} for 24 h was 1.2 %. The quantum efficiency obtained is different from that expected from very high current efficiencies of approaching 100 % for electrochemical fixation of CO_2 which was previously reported.[29a] The difference is attributed to the difference in the mode of the supply of electrons to MV^{2+}. In the case of the electrochemical fixation, the CO_2 fixation occurs with low current densities such as 50 μA cm^{-2} after MV^{2+} is reduced to methyl viologen radical cation ($MV^{+\cdot}$). The current in that case is due to the reduction of MV^{2+} that is produced from $MV^{+\cdot}$ in the CO_2 fixation reaction at the enzyme (see Fig. 1(a)) and the magnitude of the current is entirely controlled by the rate of the CO_2 fixation at the enzyme.

The situation of the photochemical fixation was quite different from that of the electrochemical fixation. Illumination at 410 nm with 0.0013 W cm^{-2} (27.8 μmol h^{-1} photons) of 0.016 mmol CdS suspended in 0.2 M TRIS buffer containing 0.12 mM MV^{2+} and 1 M triethanolamine gave the quantum efficiency of 11.1 % for the photoreduction of MV^{2+} to $MV^{+\cdot}$. Since the CO_2 fixation experiments were carried out using 1 mM MV^{2+} and not 0.12 mM MV^{2+} a quantum efficiency greater than 11.1 % is expected for the photoreduction of MV^{2+} in that case. The photoreduction of MV^{2+} in the cell used in the CO_2 fixation experiments is completed within 1.3 h with a quantum efficiency of 11.1 % and so a reduction in much shorter time is imagined for the actual experiments in which 1 mM MV^{2+} was used. The rate of regeneration of MV^{2+} from $MV^{+\cdot}$ in the course of the CO_2 fixation was 0.32 μmol h^{-1}, as deduced from the production rate of isocitrate, and was very low compared to the irradiated photons (27.8 μmol h^{-1}). Considering this, the observed low quantum efficiency for the isocitrate production seems reasonable, because a large fraction of photogenerated electrons in the 24 h illumination are not used in reducing MV^{2+}, resulting in annihilation by the recombination with positive holes.

15

There are three electron-transfer steps in the fixation reaction as shown in Fig. 1(a); between oxoglutarate and reduced ICDH, between $MV^{+\cdot}$ and oxidized ICDH, and between MV^{2+} and CdS. It is recognized from Figs. 4 and 6 that the concentration of oxoglutarate and MV^{2+} greatly influence the initial rate of isocitrate production. The concentration of oxoglutarate must affect the rate of the electron transfer between reduced ICDH and oxoglutarate, while the MV^{2+} concentration must influence the rate of the reduction of MV^{2+} and that of electron transfer between the resulting $MV^{+\cdot}$ and ICDH. The rate of the MV^{2+} reduction determined in 0.2 M TRIS buffer containing 0.1 mM MV^{2+} and 1 M triethanolamine was 0.64 μmol min^{-1}, which is ca. 70 times greater than the rate of isocitrate production (see Fig. 6), suggesting that the MV^{2+} reduction occurs rapidly in comparison with the electron transfer between ICDH and oxoglutarate and that between $MV^{+\cdot}$ and ICDH. Accordingly either one of the latter two processes must be the rate-determining step. Since the rate of the isocitrate production became constant with the [MV^{2+}] higher than 0.25 mM, the electron transfer process between reduced ICDH and oxoglutarate seems to be the rate-determining step under conditions of high concentrations of MV^{2+}.

ICDH is one of oxidoreductases,[50] and according to the reaction scheme given in Fig. 1(a), the reduced form of ICDH is oxidized in the course of the fixation of CO_2 in oxoglutarate and the resulting oxidized form is returned to the reduced form by $MV^{+\cdot}$. The reaction scheme can be formulated as shown in Fig. 8 using the ping-pong mechanisms[51] which are commonly applicable to a variety of enzyme reactions. Let ICDH, oxoglutarate, isocitrate and MV^{2+} be given by E, S, P, and M, respectively, and the suffix ox and red denote the oxidized and the reduced form, respectively. If an activated complex formed between E_{red} and S is given by $E_{red}S$ and that formed between E_{ox} and M_{red} by $E_{ox}M_{red}$, then we have the following rate equations.

16
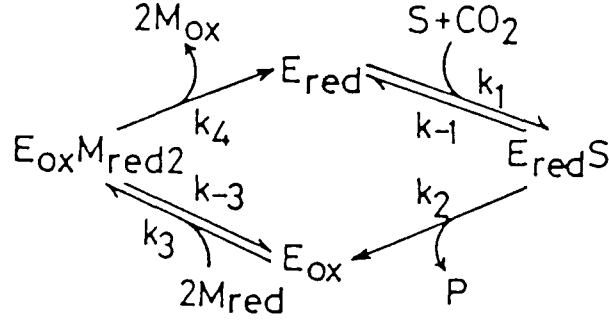
Fig. 8. Reaction scheme in the ping-pong mechanism.
E: ICDH, S: oxoglutarate, P: isocitrate, M: MV^{2+}.

$$\frac{d[E_{red}]}{dt} = -k_1[E_{red}][S][CO_2] + k_{-1}[E_{red}S] + k_4[E_{ox}M_{red2}] \tag{2}$$

$$\frac{d[E_{red}S]}{dt} = -k_2[E_{red}S] - k_{-1}[E_{red}S] + k_1[E_{red}][S][CO_2] \tag{3}$$

$$\frac{d[E_{ox}]}{dt} = k_2[E_{red}S] + k_{-3}[E_{ox}M_{red2}] - k_3[E_{ox}][M_{red}]^2 \tag{4}$$

$$\frac{d[E_{ox}M_{red2}]}{dt} = -k_4[E_{ox}M_{red2}] - k_{-3}[E_{ox}M_{red2}] + k_3[E_{ox}][M_{red}]^2 \tag{5}$$

where the bracket represents the concentration of each chemical species, and k_n is the rate constant of the reaction step given in Fig. 8. By applying the steady state conditions to these equations, we have

$$[E_{red}S] = \frac{[S][CO_2][E_{red}]}{K_1} \tag{6}$$

$$[E_{ox}M_{red2}] = \frac{[M_{red}]^2[E_{ox}]}{K_2} \tag{7}$$

17

$$[E_{ox}] = \frac{k_2 K_2 [S][CO_2][E_{red}]}{k_4 K_1 [M_{red}]^2} \tag{8}$$

where $K_1 = (k_{-1} + k_2) / k_1$ and $K_2 = (k_{-3} + k_4) / k_3$.

The total concentration of ICDH ($[E]_0$) is given by eq. (9)

$$[E]_0 = [E_{red}] + [E_{red}S] + [E_{ox}] + [E_{ox}M_{red2}] \tag{9}$$

and by inserting eqs. (6) to (8) into this equation, followed by rearrangement, we have

$$[E_{red}] = \frac{k_4 K_1 [M_{red}]^2}{k_2 K_2 [S][CO_2] + k_4 K_1 [M_{red}]^2 + (k_2 + k_4)[M_{red}]^2 [S][CO_2]} [E]_0 \tag{10}$$

The rate of the isocitrate production (v_p) is then given by

$$v_p = k_2 [E_{red}S]$$

$$= \frac{k_2 k_4 [S][CO_2][M_{red}]^2}{k_2 K_2 [S][CO_2] + k_4 K_1 [M_{red}]^2 + (k_2 + k_4)[M_{red}]^2 [S][CO_2]} [E]_0 \tag{11}$$

If the saturated concentration of CO_2 (C) is used as $[CO_2]$ in eq. (11), followed by rearrangement, we have

$$\frac{1}{v_p} = \frac{K_2}{k_4 [M_{red}]^2 [E]_0} + \frac{K_1}{k_2 C[S][E]_0} + \frac{k_2 + k_4}{k_2 k_4 [E]_0} \tag{12}$$

According to eq. (12) the maximum production rate of isocitrate (V_{max}) is obtained under the conditions of $[M_{red}] \to \infty$ and $[S] \to \infty$ at the constant concentration of ICDH. Then eq. (12) is simplified to eq. (13)

$$\frac{1}{V_{max}} = \frac{k_2 + k_4}{k_2 k_4 [E]_0} \tag{13}$$

The Michaelis-Menten constant concerning the substrate (K_{m1}) is defined as the concentration of the substrate at the half of the maximum production rate obtained at infinite concentration of M_{red} where the electron transfer between the reduced ICDH and the substrate is the rate-limiting step in the production of isocitrate. By substituting $[M_{red}] \to \infty$ and $v_p = V_{max}/2$ into eq. (12), followed by rearrangement with the use of eq. (13), we obtain

$$[S] = \frac{k_4 K_1}{(k_2 + k_4)C} = K_{m1} \qquad (14)$$

Similarly, the Michaelis-Menten constant concerning $[M_{red}]$ (K_{m2}) is obtained by substituting $[S] \to \infty$ and $v_p = V_{max}/2$ into eq. (12).

$$[M_{red}] = \left(\frac{k_2 K_2}{k_2 + k_4} \right)^{1/2} = K_{m2} \qquad (15)$$

The substitution of eq. (14) and eq. (15) in eq. (12), followed by rearrangements gives

$$\frac{1}{v_p} = \frac{1}{V_{max}} \left[\frac{K_{m1}}{[S]} + \left(\frac{K_{m2}}{[M_{red}]} \right)^2 + 1 \right] \qquad (16)$$

Considering that the concentration of $MV^{+ \cdot}$ $([M_{red}])$ can be regarded as that of MV^{2+} due to rapid reduction and the rate of the isocitrate production becomes constant at concentrations greater than 0.25 mM, one can regard $[M_{red}]$ as being infinite under the present experimental conditions. Accordingly, the second term in eq. (16) can be neglected in the experiments shown in Figs. 3 and 4 where the concentration of MV^{2+} was 1 mM.

Plots of v_p^{-1} as a function of $[S]^{-1}$ with the use of the results shown in Fig. 4 give Fig. 9(a), from which V_{max} is obtained as the value of v_p at $[S]^{-1}=0$, and then K_{m1} is obtained from the slopes of the plots. Similarly, K_{m2} is estimated from the slopes of $[M_{red}]^{-2}$ vs. v_p^{-1} plots (Fig. 9(b)) with the use of the results shown in Fig. 6. V_{max}, K_{m1} and K_{m2} determined in this way were 2.49 μmol h^{-1}, 23.9 mM and 0.030 mM, respectively. The values obtained here support the views described above that the electron transfer between reduced ICDH and the substrate is the rate-determining step except where the MV^{2+} concentration is very low. The applicability of eq. (16) was confirmed by inserting the determined V_{max}, K_{m1}, and K_{m2} value into this equation for a variety of concentrations of the substrate and the mediator. The dashed lines given in Figs. 4 and 6 are the results obtained by using eq. (16), and it is found

19

that the dashed curves fit very well in the experimental results.
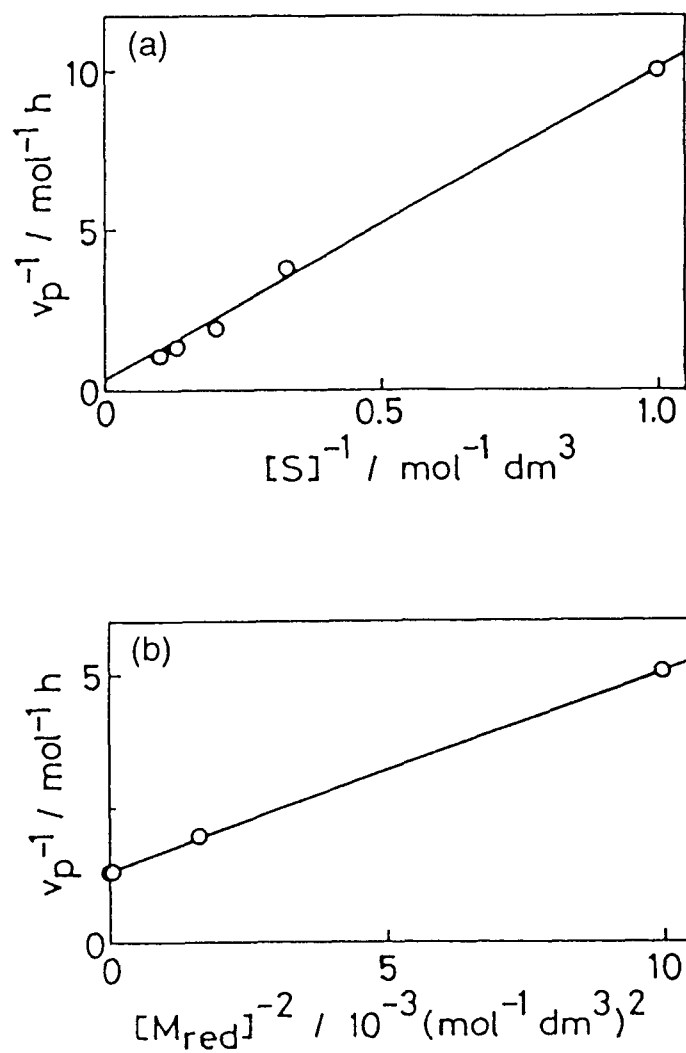
Fig. 9. (a) v_p^{-1} vs. $[S]^{-1}$ plots using the results shown in Fig. 4. (b) v_p^{-1} vs. $[M_{red}]^{-2}$ plots with the use of the results shown in Fig. 6 and the K_{m1} and V_{max} obtained.

1-3-2 Photochemical Fixation of Carbon Dioxide in Pyruvate Using 2-Mercaptoethanol as a Hole Scavenger

Figure 10 shows the time course of malate production obtained in 10 cm^3 of CO_2-saturated TRIS buffer solution. The solution composition is given in the figure caption. Illumination of these suspensions resulted in the selective production of malate in proportion to the illumination time for the first few hours. No other reduction products of CO_2 were detected. If the

Fig. 10. Time course of malate production at (a) TiO_2/clay and (b) CdS photocatalysts. The solution was a CO_2-saturated TRIS buffer solution (10 cm^3) containing 1 mM MV^{2+}, 0.1 mM $NADP^+$, 0.2 unit of FNR, 1 unit of ME, 2 mM pyruvate, 27 mM 2-mercaptoethanol and 1.25 mM TiO_2/clay or 1.25 mM CdS. Turnover number of ME in the malate production is also given.

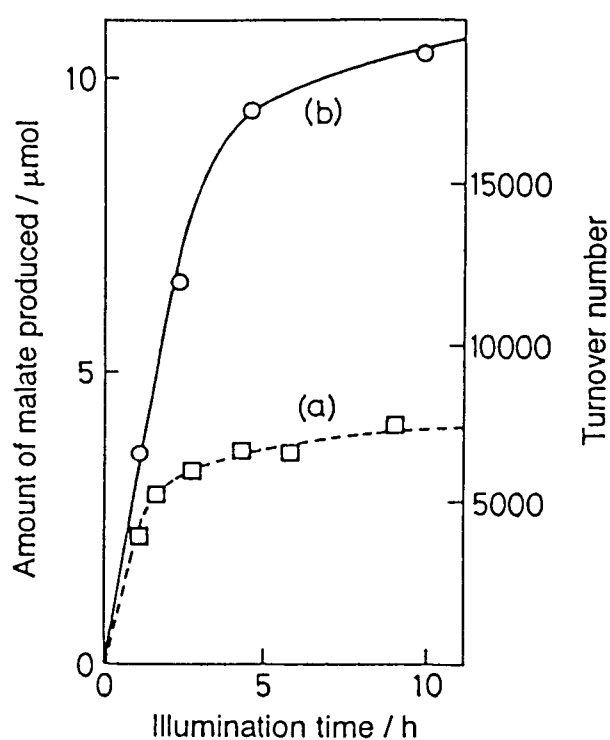semiconductor photocatalysts were eliminated from the reaction solution containing MV^{2+}, FNR, $NADP^+$, ME and hole scavenger, malate was not produced, suggesting that the semiconductor photocatalysts are essential for the production of malate. In Fig. 10 the turnover number of the enzyme is also given. For this estimation, we need the number of moles of active sites per one ME molecule, which was estimated to be 5.5×10^{-10} mol with assumption that the molar mass of ME extracted from chicken liver is 2.6×10^5, one ME molecule contains four active center-subunits[52,53] and one unit of ME contains 3.6×10^{-5} g of ME protein.[52,53] The turnover number obtained was very large.

Malate production became stagnated with illumination times greater than 5 h for the CdS suspension and greater than 1.5 h for the TiO_2/clay suspension. It is thought that at these stages, ca. 50 % of pyruvate was converted to malate at CdS and ca. 15 % at the TiO_2/clay. It is therefore unlikely that the observed stagnation resulted from a deficiency of the substrate. If 1.25 mM TiO_2/clay was suspended in an aqueous solution containing 0.2 mM MV^{2+} and 27 mM 2-mercaptoethanol and then illuminated by an Hg arc lamp ($\lambda > 310$ nm), the $MV^{+\cdot}$ production was completed after illumination for ca. 10 min. Since 1 mM MV^{2+} was used in the above-described photochemical fixation of CO_2 in pyruvate, the reduction of MV^{2+} must have been completed after illumination for 50 min. However, since the stagnation of the malate production appeared with illumination for 1.5 h for the case of using the TiO_2/clay photocatalyst, as shown in Fig. 10(a), it is concluded that this does not result from the stagnation of $MV^{+\cdot}$ production. Why the malate production was stagnated with an increase in the illumination time is a matter for discussion. There may be at least two causes. (i) the photodegradation of ME and (ii) the predominance of the back reaction of the enzymatic CO_2 fixation at ME due to the reaction equilibrium:

22

$$\text{pyruvate} + CO_2 + NADPH + H^+ \rightleftharpoons \text{malate} + NADP^+ \tag{17}$$
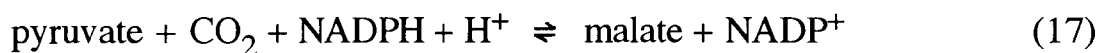
To clarify which is responsible, 1 unit of fresh ME was added to the reaction solution at the time when a noticeable stagnation was observed, e.g. 5 h at TiO_2/clay. The malate production then began to occur again, suggesting that the degradation of ME, rather than the equilibrium of the enzymatic CO_2 fixation reaction at ME (see Fig. 1(b)) is responsible for the observed stagnation of the malate production. It is more likely that ME was gradually degraded by photoinduced oxidation at the photocatalyst surfaces. In contrast, the addition of FNR or $NADP^+$ or the both did not result in any appreciable improvement in the malate production. These results suggest that incomplete regeneration of $NADP^+$, if any, was not responsible for the stagnation of the malate production.

If the amount of malate is obtained as a function of illumination time for several concentrations of pyruvate and the rate of malate production is estimated at an initial stage of the illumination, then the rate of malate production is related to the concentration of pyruvate, as shown in Fig. 11. Similar relations were obtained at the CdS photocatalyst. In the case of the TiO_2/clay photocatalyst, the rate of the malate production was proportional to the concentration of pyruvate up to 1 mM, beyond which the rate became saturated. It is then thought that below 1 mM of pyruvate, enzymatic fixation of CO_2 at ME (see Fig. 1(b)) must be the rate-determining step. For the concentrations greater than 1 mM, one of the other four electron transfer steps constituting the photochemical enzymatic fixation process of CO_2 (see Fig. 1(b)) should be rate-determining.

In order to clarify the rate-determining step the influence of the amounts of ME, FNR and $NADP^+$ on the rate of the malate production was investigated at fixed concentrations of pyruvate and MV^{2+} of 2 mM and 1 mM, respectively. An increase of ME from 1 unit to 5 units or $NADP^+$ from 0.1
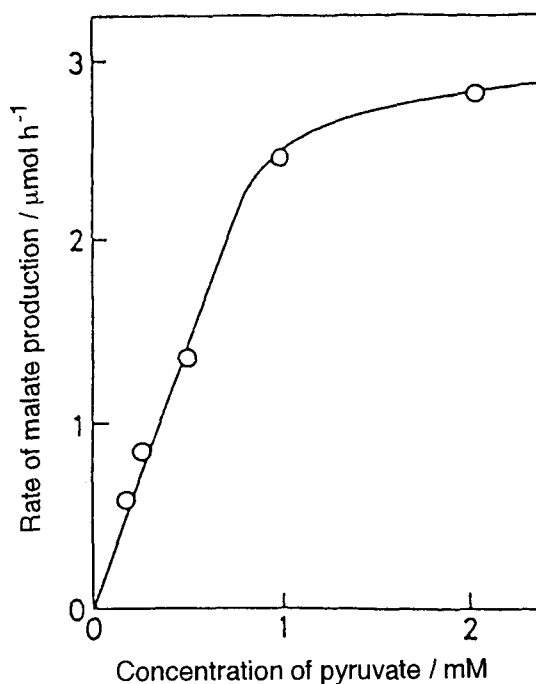
23

Fig. 11. Rate of malate production at the TiO_2/clay photocatalyst as a
function of the concentration of pyruvate.

to 0.2 mM did not increase the rate of malate production, while an increase of

FNR from 0.2 to 1 unit resulted in 2.2 times increase in the rate of malate

production.   Therefore it is concluded that the electron transfer between

$MV^{+ \cdot}$ and FNR is the rate-determining step.   The apparent quantum

efficiencies for the malate production determined for 1.25 mM photocatalysts

in the presence of 1 mM MV^{2+}, 0.08 unit of FNR, 0.1 mM $NADP^+$, 0.4 unit

of ME, and 2 mM pyruvate were 9.7 % for the use of TiO_2/clay and 0.9 % for

the CdS.   In the case of using the former photocatalyst, NADPH also absorbs

the monochromatic light.   Since the absorbance at 313 nm of 0.1 mM NADPH

was one tenth that of 1.25 mM TiO_2/clay photocatalyst, it is thought that 90 %

of the irradiated photons must have been used in the photo-excitation of the

TiO_2/clay.   Then the net quantum efficiency in the use of the TiO_2/clay would

24

be 10.7 %. One may think from the results shown in Fig. 10 that the CdS photocatalyst should give a higher quantum efficiency than the TiO_2/clay. However, the light source used in the experiments was different, and the absorption threshold of the semiconductor photocatalysts was different. The low quantum efficiency obtained at the CdS photocatalyst was improved slightly to 2.5 % if the amount of suspended photocatalyst was increased to 6.25 mM.

Judging from results reported for TiO_2 photocatalysts,[54] pyruvate used as a substrate may be reduced to lactate. This was found to be true at the TiO_2/clay photocatalyst if the concentration of the photocatalyst was increased from 1.25 to 6.25 mM without changing the concentration of MV^{2+} (1 mM). The reduction of pyruvate must take place if the concentration of MV^{2+} becomes in a relative sense, too small to be reduced selectively at the photocatalyst surface. As long as the concentration of the photocatalyst was kept 1.25 mM in the presence of 1 mM MV^{2+}, MV^{2+} alone was photoreduced, allowing the selective fixation of CO_2 in pyruvate.

As described above, the photochemical fixation of CO_2 in pyruvate at TiO_2/clay and CdS photocatalysts occurred with the quantum efficiency of 10.7 and 0.9 %, respectively. On the other hand if the quantum efficiencies for photoreduction of MV^{2+} to $MV^{+\cdot}$ were obtained under the same experimental conditions, but in the absence of $NADP^+$, FNR and ME, they were 16.4 % for TiO_2/clay and 8.3 % at the CdS. The obtained quantum efficiencies for the $MV^{+\cdot}$ production were much higher than that for malate production, giving support to the above-described view that the rate-determining step is not the reduction of MV^{2+} to $MV^{+\cdot}$ but the electron transfer between $MV^{+\cdot}$ and FNR. It was found that the illumination intensity greatly influences the quantum efficiency for malate production, and the smaller the illumination intensity, the larger the quantum efficiency. For

example, the quantum efficiencies obtained under the same solution conditions as described above except for the concentration of the CdS photocatalyst which was 6.25 mM were 2.5, 4.8 and 5.6 % for the illumination intensities of 1.73 $\times 10^{-3}$, 1.61×10^{-4} and 2.59×10^{-5} W cm^{-2}, respectively.

1-3-3 Photochemical Conversion of Lactate to Malate through Pyruvate

As shown above, the quantum efficiency for malate production at the CdS photocatalyst was smaller than that at the TiO_2/clay photocatalyst. However, the use of the CdS photocatalyst is preferred from the viewpoint that lactate is photooxidized to pyruvate. This photooxidation reaction did not occur at the TiO_2/clay.

Figure 12 shows the time course of the photoreduction of MV^{2+} and photooxidation of lactate to pyruvate on the CdS photocatalyst, which was obtained in CO_2-saturated TRIS buffer containing MV^{2+}, lactate, and CdS. No other products were obtained by the photooxidation of lactate. Photogenerated electrons must be used in reducing MV^{2+} to $MV^{+\cdot}$, while photogenerated holes must be used in oxidizing lactate to pyruvate.

$$2MV^{2+} + 2e^- \longrightarrow 2MV^{+\cdot} \tag{18}$$

$$CH_3CHOHCOO^- + 2h^+ \longrightarrow CH_3COCOO^- + 2H^+ \tag{19}$$
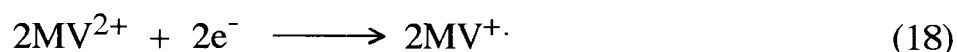
According to the results given in Fig. 12, the rate of $MV^{+\cdot}$ production was twice that of pyruvate, satisfying the chemical stoichiometry for the light-induced reaction.

When FNR, NADP$^+$ and ME were added to the above solution, both pyruvate and malate were produced, as shown in Fig. 13, suggesting that a fraction of the photo-produced pyruvate was converted to malate by the enzymatic CO_2 fixation. However, the amount of the malate produced was ca.
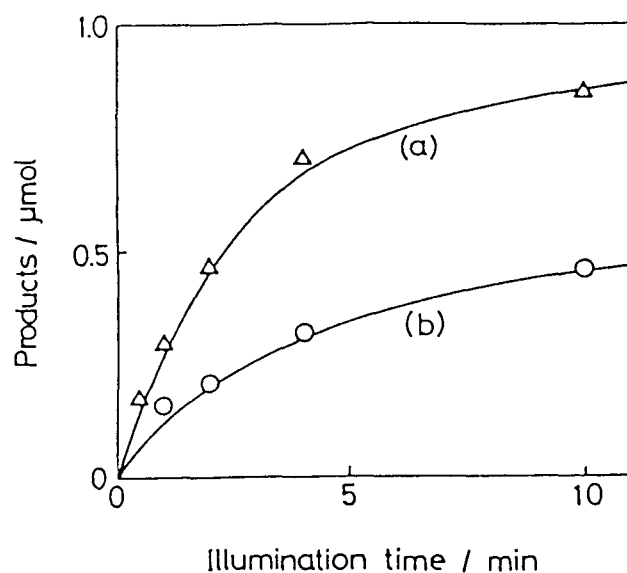
Fig. 12. Time course of the production of (a) $MV^{+\cdot}$ and (b) pyruvate under illumination by a Xe arc lamp. The solution was a CO_2-saturated TRIS buffer solution (4 cm^3) containing 0.25 mM MV^{2+}, 100 mM lactate and 1.25 mM CdS.
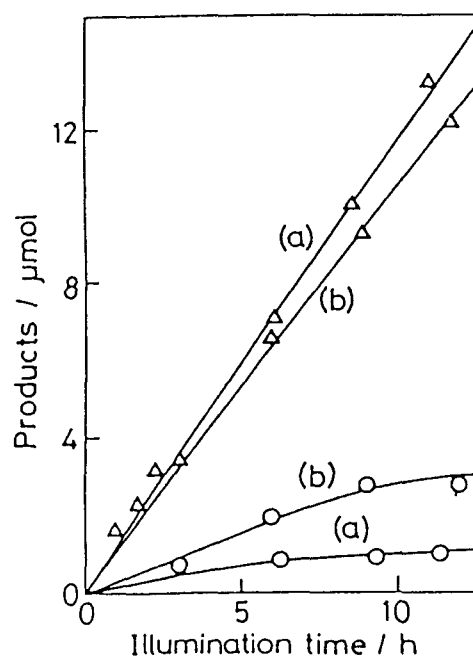
Fig.13. Time course of the photoproduction of ($\triangle$) pyruvate and ($\bigcirc$) malate in the presence of (a) 1 unit and (b) 5 units of ME in a CO_2-saturated TRIS buffer solution (10 cm^3) containing 1 mM MV^{2+}, 0.2 unit of FNR, 0.1 mM $NADP^+$, 100 mM lactate and 1.25 mM CdS.

1 μmol at most even after 10 h of the illumination, which is much smaller than that achieved when using 2-mercaptoethanol as the hole scavenger. The result suggests that lactate exerts a negative effect on the enzymatic CO_2 fixation reaction. To confirm this view the effect of lactate on the catalytic activities of ME and FNR was investigated.

It is expected that in the enzymatic fixation of CO_2 in pyruvate NADPH is oxidized to $NADP^+$ at ME with the consumption of two electrons and the release of one proton (see Fig. 2). The decrease in NADPH concentration was experimentally confirmed, as shown by the time course given in Fig. 14(b). NADPH concentration steadily decreased if the solution did not contain lactate. However, in the presence of 100 mM lactate the rate of decrease of the NADPH concentration was very low (Fig. 14(a)).

According to the reaction scheme given by Fig. 2, $NADP^+$ is reduced to NADPH with consumption of two electrons from two $MV^{+·}$ and one proton.
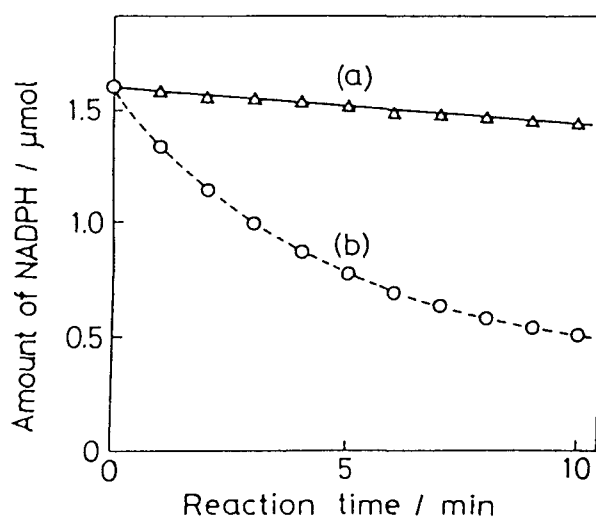

Fig. 14. Time course of the consumption of NADPH in the presence (a) and the absence (b) of 100 mM lactate, obtained after 1 unit of ME was added to a CO_2-saturated TRIS buffer solution (4 cm³) containing 2 mM pyruvate and 0.4 mM NADPH.

Fig. 15 confirms this result, where the time course of the production of NADPH is given. The results were obtained for 4 cm^3 of CO_2-saturated TRIS buffer solution containing MV^{2+}, FNR, CdS and 2-mercaptoethanol as a hole scavenger in the presence and absence of lactate. It is seen in Fig. 15 that lactate retards a little the reduction of $NADP^+$ to NADPH. By comparing the results shown in Fig. 14 with those in Fig. 15 it is concluded that lactate has a more serious effect on ME than on FNR.

As mentioned above, lactate has unfavorable effects on the activities of ME and FNR, especially on the former. This imposes a serious limitation in the light-induced enzymatic production of malate from lactate. However, the unfavorable effect of lactate on ME may be weakened by appropriately choosing the relative concentrations of these substances, as the results shown in Fig. 13 suggest. In that case, the use of 5 units of ME resulted in a greater amount of malate with less suppression of the pyruvate production than in the
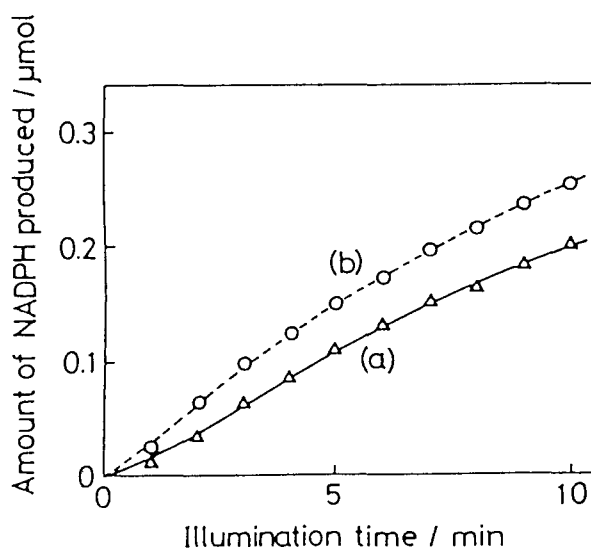

Fig. 15. Time course of the production of NADPH in the presence (a) and absence (b) of 100 mM lactate in a CO_2-saturated TRIS buffer solution (4 cm^3) containing 0.3 mM MV^{2+}, 0.4 mM $NADP^+$, 0.1 unit of FNR, 1.25 mM CdS and 27 mM 2-mercaptoethanol.

use of 1 unit of ME.

1-4   Summary

The photochemical fixation of CO_2 in oxoglutarate and pyruvate to yield isocitrate and malate have been achieved using CdS particle suspensions and TiO_2 microcrystal as photocatalysts, ICDH and ME as the catalyst, MV^{2+} as the electron mediator and triethanolamine, 2-mercaptoethanol or lactate as the hole scavenger.   The rate of isocitrate and malate production depended on the concentration of the substrate and the mediator.   It was concluded that the rate-determining step for the photochemical fixation of CO_2 in oxoglutarate and pyruvate was the electron transfer between ICDH and substrate and that between $MV^{+\cdot}$ and FNR, respectively.   The use of lactate as the hole scavenger resulted in the selective photoproduction of pyruvate at the CdS photocatalyst, a fraction of which was then converted into malate by reductive CO_2 fixation at the malic enzyme.   Lactate exerted unfavorable effects especially on the catalytic activities of ME, but the increase of the amount of ME reduced these negative effects.

Chapter 2 Effect of Particle Size of Semiconductor Microcrystals on Photocatalytic Activities for Carbon Dioxide Reduction

2-1 Introduction

Light-induced reductions of CO_2 molecules in aqueous solutions using semiconductor photocatalysts have been investigated fairly intensively.[1-18] Not only two-electron reduction products such as carbon monoxide and formate but also four and six-electron reduction products such as formaldehyde and methanol have been reported. However, most of the results reported so far are unsatisfactory from the viewpoint of the quantum efficiency. Recent studies on semiconductor photocatalysis have revealed that such small semiconductor particles as to show the size quantization effect possess high photocatalytic activities. For instance, TiO_2 microcrystals[46,55,56] and Fe_2O_3 microcrystals[33] showed the enhanced photocatalytic activity in comparison with the bulk semiconductors for the photo-Kolbe reaction, photooxidation of alcohol and photo-hydrogenation of propyne. Accordingly, it is of very interest to clarify relations between the photocatalytic activities for CO_2 reduction and particle size of the semiconductor microcrystalline photocatalysts. For this purpose, ZnS and TiO_2 microcrystalline photocatalysts were used in the present experiments. The conduction band potentials of ZnS and TiO_2 bulk semiconductors are -2.09 V vs. SCE[57] and -0.70 V vs. SCE[58] at pH 7, respectively, which are able to reduce CO_2. In addition, TiO_2 is an effective photocatalyst for reducing CO_2 to multielectron reduction products such as formaldehyde, methanol and methane.[2-5,9,10,59] For example, Anpo et al.[59] prepared TiO_2 microcrystals on vycor glass surfaces by using hydrolysis reactions of hydroxyl groups of

this support with $TiCl_4$ and then examined its activities for photoreduction of CO_2. They discovered that the prepared TiO_2 microcrystals showed high activities for photoreduction of CO_2 in the presence of water vapor. They obtained methane, methanol and CO as the reduction products of CO_2. The production ratio of these products was dependent on the reaction conditions, though the quantum efficiency for their production was not determined. In this chapter, the quantum efficiency was evaluated as a measure of the photocatalytic activities for the CO_2 reduction.

2-2   Experimental

Chemicals

Zinc perchlorate (Kishida), sodium sulfide, sodium iodide, 2-propanol, ethanol, sodium bicarbonate (Wako), titanium tetraethoxide ($Ti(OEt)_4$), silicon tetraethoxide ($Si(OEt)_4$) (Nacalai Tesque), SiO_2 powder (Japan Aerosil, 200CF, surface area: 200 m^2 g^{-1}) and TiO_2 powder (Japan Aerosil, surface area: 50 m^2 g^{-1})were used as received.

Procedure

The preparation of ZnS photocatalysts and experiments on photoreduction of CO_2 were basically followed to those reported by Henglein et al.[17]   0.1 M NaOH was added to 50 cm^3 of 0.4 to 1.2 mM $Zn(ClO_4)_2$ in the presence of 12 mM SiO_2 powder in such a way that the number of mole of NaOH was twice that of Zn^{2+}. The specific surface area of the SiO_2 used as a stabilizer was 200 m^2g^{-1}. Then 50 cm^3 of 0.4 mM Na_2S was added to the above solution to produce ZnS colloids. These procedures were carried out under N_2.

TiO_2 microcrystals prepared in SiO_2 matrices, which are denoted as Q-TiO_2/SiO_2 below, were prepared in the following way; Aqueous ethanol

solution (8%(v/v) of water) containing 1 M HCl was added to ethanol solution containing $Si(OEt)_4$ and $Ti(OEt)_4$ of various mole ratios at an equal volume, resulting in sols consisting of TiO_2 and SiO_2. The total concentration of $Ti(OEt)_4$ and $Si(OEt)_4$ was 0.55 M after the mixing. After stirring for 3 h, 1.6 cm^3 of the sol was casted on quartz glass plates (7.6 cm×2.6 cm). By being dried in a desiccator, transparent gel films of Q-TiO_2/SiO_2 were produced. This transparent films were stripped off from the quartz plate and dried in vacuo at 120 ^oC for 2 h to give transparent flake films. On the other hand, bulk TiO_2/SiO_2 mixtures with same composition ratio as Q-TiO_2/SiO_2 flakes were prepared by mixing the commercially available TiO_2 and SiO_2 powders.

The procedure of the photoreduction experiments of CO_2 using ZnS microcrystalline colloids was a little different from that using Q-TiO_2/SiO_2. In the case of the ZnS microcrystals, the resulting ZnS colloids were aged for a day, and then 0.32 cm^3 of 2-propanol was added as a hole scavenger to 4 cm^3 of the ZnS colloid which was put in a quartz reaction cell of 6.8 cm^3 capacity. The adjustment of pH in the ZnS colloid was done by adding appropriate amounts of $NaHCO_3$. Illumination of CO_2-filled ZnS colloids was made by a 500 W high pressure Hg arc lamp through 0.1 M sodium iodide solution to cut off UV lights of wavelengths shorter than ca. 270 nm. On the other hand, as for Q-TiO_2/SiO_2, the photoreduction experiments of CO_2 were carried out using a quartz cell of 1.6 cm diameter and 5 cm height. Q-TiO_2/SiO_2 flakes and bulk TiO_2/SiO_2 mixtures prepared with different Ti/Si mole ratios were added to 4 cm^3 of 1 M 2-propanol aqueous solution in such a way as to give 50 mmol of TiO_2. After bubbling CO_2 for 30 min, the pH of the solution was 3.2. Lights from a 500 W high pressure Hg arc lamp were passed through a UV-29 cut off filter (Toshiba) to cut off wavelengths shorter than 270 nm and illuminated from the bottom of the cell. During the illumination, the solution

was not stirred to prevent destruction of the flakes, which might cause light scattering.

Determination of Products

Hydrogen and carbon monoxide produced in the gas phase were determined by a G-180 gas chromatograph (Yanaco) equipped with a molecular sieve 5A column (GL Sciences) and a TCD detector using argon as a carrier gas for the former and helium for the latter. Methane and ethylene produced in the gas phase were determined by a G-180 gas chromatograph equipped with a Porapak Q column (GL Sciences) and an FID detector using argon as a carrier gas. Acetone produced in the liquid phase was determined by a Model 802 gas chromatograph (Okura) equipped with a BX-10 column (GL Sciences) and a FID detector. A CCPD high pressure liquid chromatograph (Tosoh) equipped with an organic acid column (Waters) and a UV-8000 UV detector (Tosoh) were used to determine formate produced.

The quantum efficiency for photocatalytic reduction of CO_2 to formate, methane and ethylene was determined based on the amount produced by illumination for 8 h at 280 nm which was obtained by using a CT-10 monochromater or an interference filter (Oriel 280BP11), and the number of photons determined by ferrioxalate actinometry. In the determination of the number of photons absorbed in the photocatalyst, that transmitted through the cell was evaluated and subtracted from that of incident photons.

2-3 Results and Discussion

2-3-1 Effect of Particle Size of Zinc Sulfide Microcrystals on Photocatalytic Activities for Carbon Dioxide Reduction

The absorption threshold shifted to short wavelengths with an increase in the $[Zn^{2+}]$ / $[S^{2-}]$ ratio in the preparation of the ZnS colloids, as shown in Fig. 16. All spectra had pronounced shoulders characteristics of excitons.

Photoreduction of CO_2 at pH 7 in the presence of 2-propanol resulted in formate, hydrogen and acetone, as shown in Fig. 17. No other products were produced. The last substance was produced by oxidation of 2-propanol. The results satisfied chemical stoichiometry in the photocatalytic reaction. Since the production of those substances occurred linearly with illumination time,
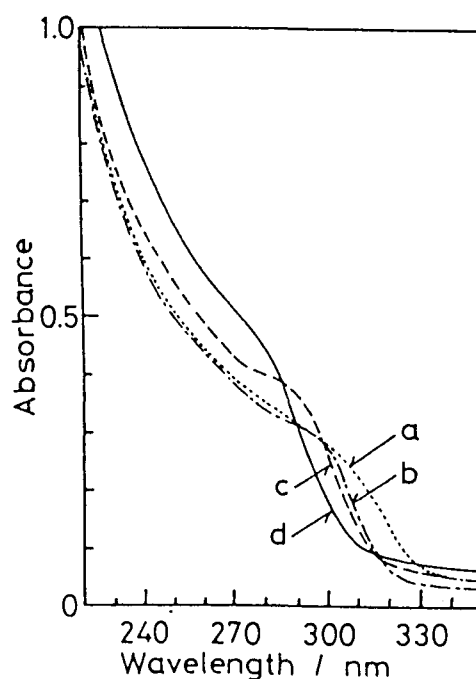
Fig. 16. Absorption spectra of ZnS colloids prepared with different $[Zn^{2+}]$ / $[S^{2-}]$ ratios, taken after aging for a day.
$[Zn^{2+}]$ / $[S^{2-}]$: (a) 1.0, (b) 1.25, (c) 1.5, (d) 3.0.

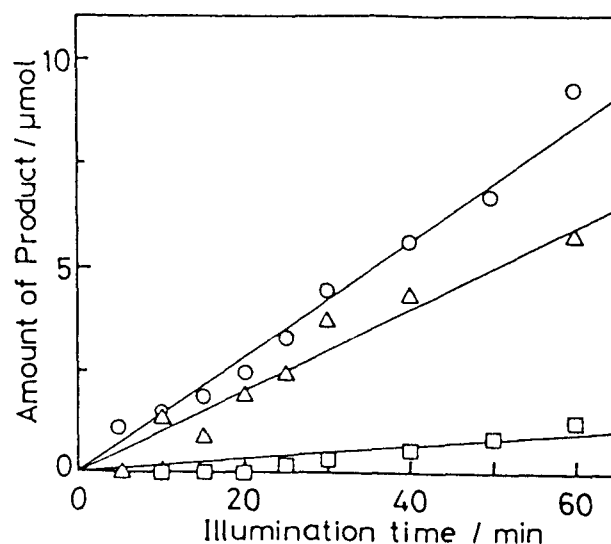Fig. 17. Time courses of productions of ($\triangle$) formate, ($\square$) hydrogen and ($\bigcirc$) acetone. $[Zn^{2+}] / [S^{2-}]$ ratio is 1.5. Solution pH is 7.

the activity of the ZnS microcrystals is said to have been invariable during the course of the photocatalytic reaction. It was found that there was a tendency for the production rate of formate to increase with decreasing the solution pH, but the decrease in pH caused instability of the ZnS colloids. Then in the following experiments the reaction solutions were kept at pH 5.2.

The quantum efficiencies for the formate production (Φ) were increased by increasing the $[Zn^{2+}] / [S^{2-}]$ ratio in the preparation of ZnS colloids, as shown by curve a of Fig. 18. Curve b of Fig. 18 gives the bandgap values of the ZnS microcrystals in the colloids as a function of the $[Zn^{2+}] / [S^{2-}]$ ratio. The determination of the bandgap energy (E_g) was made by applying absorption spectrum of each photocatalyst given in Fig. 1 to the following equation.

$$\sigma h\nu = A (h\nu - E_g)^{n/2} \tag{20}$$

where σ is the absorption coefficient and $h\nu$ is the photon energy. Since ZnS is a semiconductor of direct bandgap transition, $n=1$ holds. The bandgap
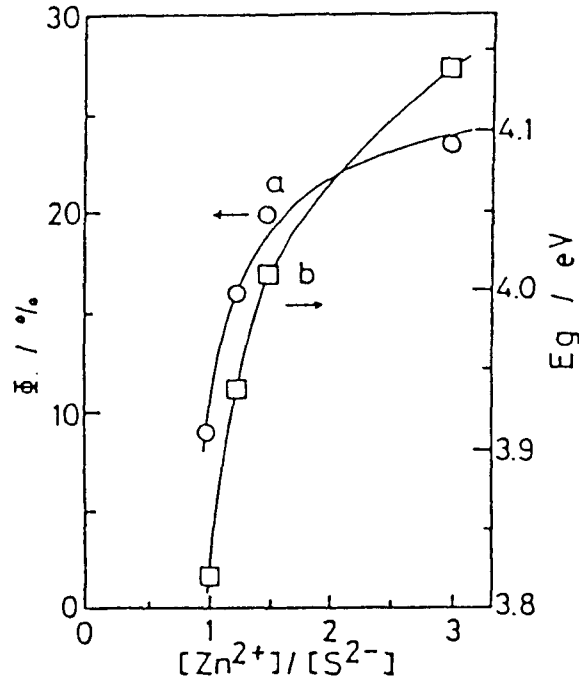
36

Fig. 18. Effects of $[Zn^{2+}] / [S^{2-}]$ ratio on quantum efficiencies for formate production (a) and bandgaps of the photocatalysts determined before illumination (b).

could be determined without any ambiguity by making $(\sigma h\nu)^2$ vs. $h\nu$ plots.

The particle size (d) of ZnS microcrystals used here was estimated by applying the E_g values to the following equation,[60]

$$E_g = E + \frac{2\hbar^2\pi^2}{d^2} \left(\frac{1}{m_e^*} + \frac{1}{m_h^*} \right) - \frac{3.6e^2}{\varepsilon d} \tag{21}$$

where m_e^*, m_h^*, ε and E are the effective mass of an electron and a hole, the dielectric constant of the semiconductor and the bulk band gap energy, respectively. As the value of m_e^* and m_h^* of ZnS, we adopted 0.25[61] and 0.59,[61] respectively. While 5.2[62] and $3,70$ were employed as ε and E, respectively. As a result we obtained 5.3 nm, 4.3 nm, 3.9 nm, and 3.4 nm for $[Zn^{2+}] / [S^{2-}]= 1$, 1.25, 1.5, and 3, respectively. The estimated particle sizes were in fair agreement with those evaluated from observations by a Hitachi H-

37

9000 high resolution transmission electron microscope (TEM). An example of photographs is given in Fig. 19 which was taken for ZnS microcrystals prepared with $[Zn^{2+}] / [S^{2-}] = 3$. The ZnS microcrystals are recognized as dark speckles having lattice plane images. The mean size of these ZnS microcrystals was judged to be 3.6 nm, although a relatively wide distribution of particle sizes ranging from 3 nm to 5 nm is noticed.

Curve a of Fig. 20 shows the quantum efficiency for the formate production as a function of the obtained particle size of the ZnS photocatalysts. It is found that the smaller the particle diameter of ZnS microcrystals, the greater the quantum efficiency. Then questions arise whether or not this finding resulted from differences in the surface area of the photocatalysts. To clarify this question, the quantum efficiency per unit surface area of the photocatalysts (Φ / S) was obtained. The surface area was estimated by assuming that ZnS photocatalysts were consisted of spherical particles. In curve b of Fig. 20, Φ / S is given as a function of the particle size and the Φ / S becomes high with a decrease in the particle size. Some errors must be
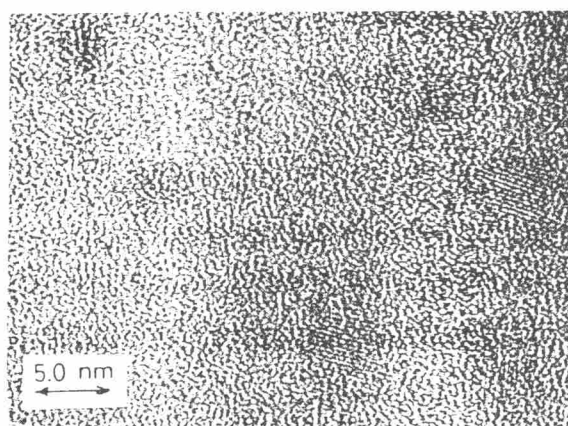

Fig. 19. High resolution TEM images of ZnS microcrystals prepared with $[Zn^{2+}] / [S^{2-}] = 3.0$.
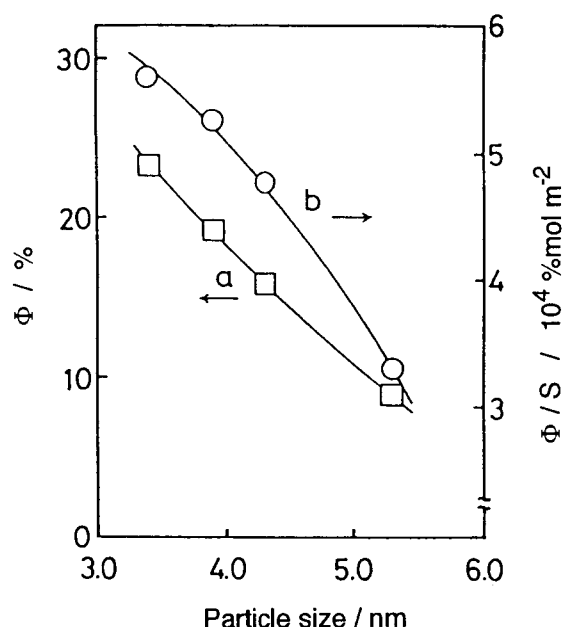
Fig. 20. (a) Φ and (b) Φ / S ratio as a function of particle size of ZnS microcrystals.

contained in the estimation in the surface area of the photocatalysts, but the result shown by curve b of Fig. 20 is significant enough to suggest that there is one important factor besides the surface area of photocatalyst for determining photocatalytic activity of ZnS. The greater the excess of $[Zn^{2+}]$ to $[S^{2-}]$, the smaller the particle diameter of the ZnS microcrystals as described above. This fact seems to suggest that the smaller the particle diameter of the ZnS photocatalyst the richer the nonstoichiometry in the photocatalyst surface, which might be favorable for adsorption of CO_2. The highest quantum efficiency for the production of formate obtained here was 30% at most and not so high as that reported by Henglein et al.,[17] but the values obtained here are high enough to confirm that size quantized ZnS is very active for photoreducing CO_2 to formate.

2-3-2 Effect of Particle Size of Titanium Dioxide Microcrystals on Photocatalytic Activities for Carbon Dioxide Reduction

Figure 21 shows absorption spectra of the $Q\text{-}TiO_2/SiO_2$ flakes prepared with different mole ratios of $Ti(OEt)_4$ and $Si(OEt)_4$. Since SiO_2 is transparent in a wavelength range given in Fig. 21, these spectra are attributable to those of the TiO_2 microcrystals. As seen in Fig. 21, absorption spectra were blue-shifted with decrease of the Ti/Si ratio. If the bandgap of TiO_2 is obtained by applying $(\alpha h v)^2$ vs. hv relation shown in eq. (20) to the spectra in their onset region, results shown by curve a of Fig. 22 were obtained. It is evident that the bandgap of TiO_2 microcrystals in the $Q\text{-}TiO_2/SiO_2$ flakes can be varied by controlling the Ti/Si ratio.

Figure 23 shows a TEM photograph and a scanning electron micrograph
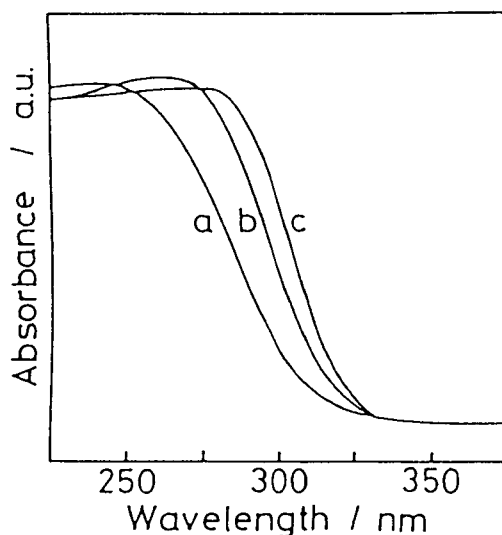

Fig. 21. Absorption spectra of $Q\text{-}TiO_2$ / SiO_2 flakes with Ti /Si ratio of (a) 0.027, (b) 0.048 and (c) 0.10.
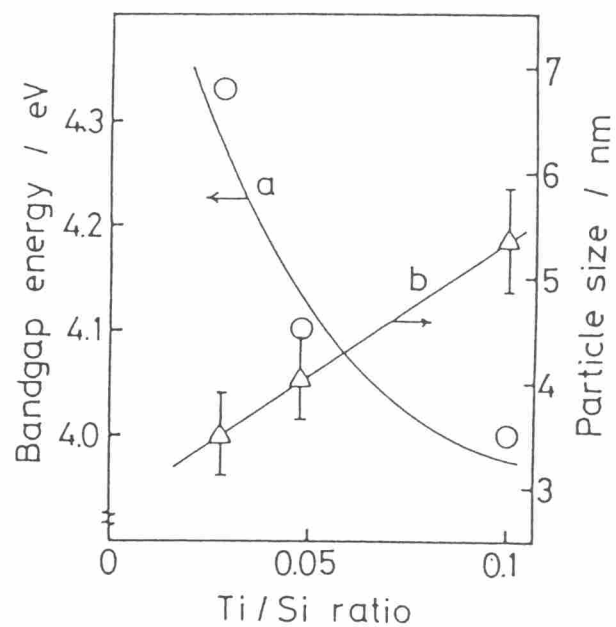
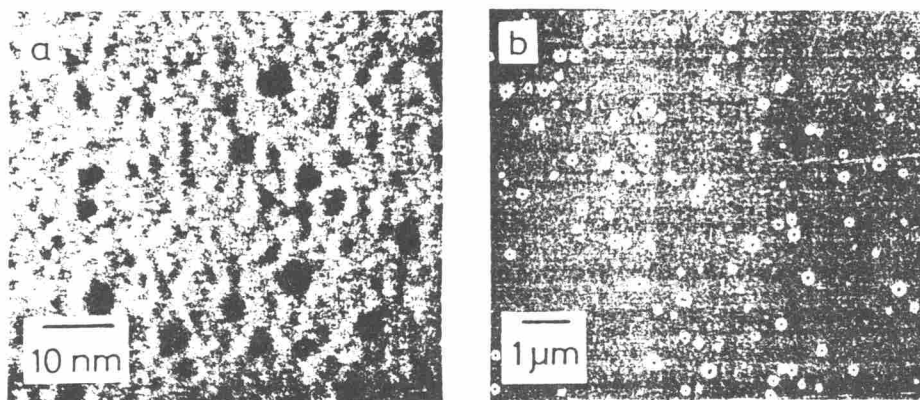Fig. 22. (a) Bandgap energy and (b) particle size as a function of Ti / Si ratio.

Fig. 23. (a) TEM and (b) SEM images of Q-TiO$_2$ / SiO$_2$ flakes. Ti / Si ratio is 0.048.

41

of the Q-TiO$_2$/SiO$_2$ flakes prepared with the Ti/Si ratio of 0.048. Black spots in the TEM photograph shows TiO$_2$ microcrystals, which were identified to be rutile from electron diffraction analysis. As shown in Fig. 23(a), TiO$_2$ microcrystals are present dispersedly in the SiO$_2$ matrices, and as Fig. 23(b) shows, there are a lot of pores in the Q-TiO$_2$/SiO$_2$ flakes. The mean particle size and the standard deviation of TiO$_2$ microcrystals in the flakes, which were obtained by counting the particles for several micrographs, are shown by curve b of Fig. 22 as a function of the T /Si ratio. The mean particle size decreases with decrease of the Ti/Si ratio, the results being in conformity with the results of the bandgap variation given by curve a of this figure. The SiO$_2$ matrices provide a good support for preventing aggregation of Q-TiO$_2$ particles.

The prepared Q-TiO$_2$/SiO$_2$ flakes worked effectively as photocatalysts for the photoreduction of CO$_2$ in 2-propanol. Figure 24(a) shows the time course of the production of reduction and oxidation products. Formate was produced as a major product of the CO$_2$ reduction with methane and ethylene as minor products. If either CO$_2$ or the Q-TiO$_2$/SiO$_2$ photocatalyst was absent, none of these products were obtained. It is recognized from the observed photocatalytic activities of the TiO$_2$/SiO$_2$ flakes that the TiO$_2$ microcrystals were not completely covered with SiO$_2$.

Furthermore, the color of the flakes gradually changed into purple during the course of the photoreduction experiments of CO$_2$. An electron spin resonance (ESR) measurement of the purple-colored Q-TiO$_2$/SiO$_2$ flakes at 77 K gave a spectrum of g=1.96,[63] evidencing the photo-formation of Ti^{3+} species. Figure 24(b) shows the time course of the Ti^{3+} production determined from the ESR measurements using 1,1'-diphenyl-2-picrylhydrazyl as a standard reference compound.

The chemical stoichiometry of the reduction and oxidation products was
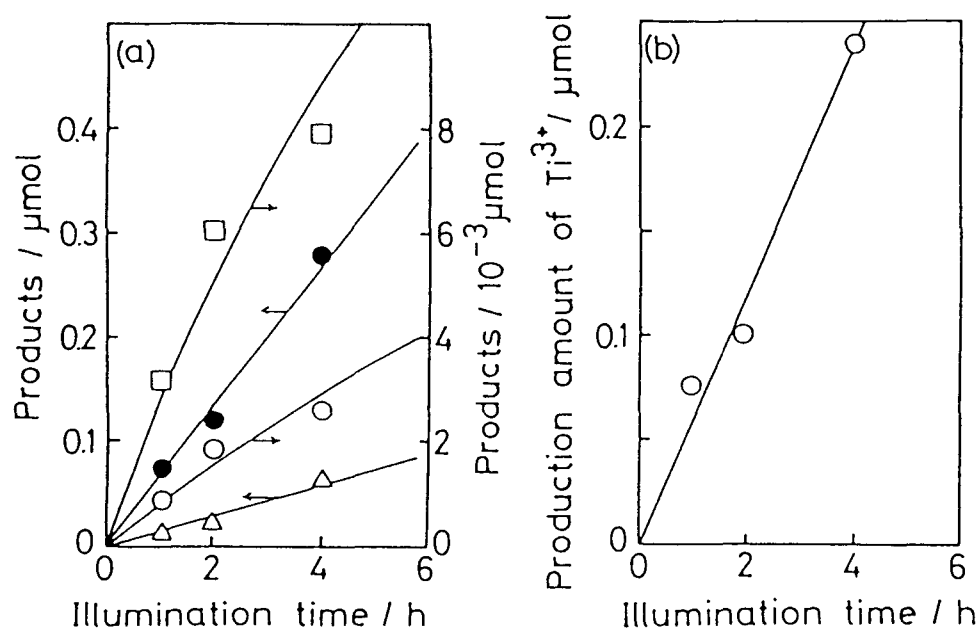
Fig. 24. (a) Time course of the production of ($\triangle$) formate, (O) methane, ($\square$) ethylene and ($\bullet$) acetone and (b) time course of Ti^{3+} production. Ti / Si ratio is 0.10.

satisfied. Table 1 shows the quantum efficiency obtained for the reduction products of CO_2 at 280 nm for three different Ti/Si ratios. As seen in this table, the $Q\text{-}TiO_2/SiO_2$ flakes showed higher quantum efficiencies for the formate and methane production than bulk TiO_2/SiO_2 mixtures of the same Ti/Si ratio. Furthermore the bulk TiO_2/SiO_2 mixture did not show activities for the production of ethylene. The quantum efficiencies obtained at the Q-TiO_2/SiO_2 flakes for the formate, methane and ethylene productions increased with a decrease of the Ti/Si ratio. Anpo et al.[59] found by ESR measurements that when methane production occurred from CO_2 in the presence of water vapor over microcrystalline TiO_2 photocatalysts anchored on vycor glass, carbon radicals and hydrogen atoms were produced as reaction intermediates. ESR measurements of $Q\text{-}TiO_2/SiO_2$ flakes (Ti/Si ratio = 0.10) did not give any

Table 1. Quantum efficiency at 280 nm for reduction products obtained in photoreduction of CO_2 in the presence of 1 M 2-propanol on $Q\text{-}TiO_2$ / SiO_2 and bulk TiO_2 / SiO_2 photocatalysts having various Ti / Si ratios

Sample	Ti / Si ratio	Quantum efficiency / %		
		HCOO⁻	CH_4	C_2H_4
$Q\text{-}TiO_2$ / SiO_2	0.10	9.0	0.50	0.15
	0.048	12.7	1.5	1.8
	0.027	14.2	3.4	2.3
bulk TiO_2 / SiO_2	0.10	5.0	0.019	0
	0.048	4.2	0.061	0
	0.027	2.4	0.030	0

signals due to carbon radicals and hydrogen atoms, suggesting that hydrocarbons produced here may proceed via other mechanisms. Furthermore, the results obtained in this study were different in terms of the kind of products. Anpo et al.[59] obtained methane, methanol and CO as the photoreduction products of CO_2, while formate was obtained here as the major products. Such a difference in the kind of products may have resulted from difference in the kind of hole scavengers used. As another cause, the difference in the experimental conditions using either a gas phase or a liquid phase might be responsible.

2-4 Summary

The absorption threshold shifted to short wavelengths with increasing the mole ratios of Zn^{2+} to S^{2-} in the preparation of ZnS microcrystals, suggesting the decrease of the particle size of the microcrystals with increasing the mole ratio. In addition, different mole ratios of Zn^{2+} to S^{2-} exhibited the different

activities for the photoreduction of CO_2, and the greater the mole ratio of Zn^{2+} to S^{2-} the higher the quantum efficiency for formate production. The size of TiO_2 microcrystals embedded in SiO_2 matrices, which were prepared using a mixed sol of TiO_2 and SiO_2 in ethanol, decreased with a decrease of the mole ratio of TiO_2 to SiO_2 in the sol. The prepared TiO_2 microcrystals showed activities for photoreduction of CO_2 to formate, methane and ethylene, and the quantum efficiencies for the production of these increased with decreasing the size of the TiO_2 microcrystals.

Chapter 3   Effect of Metal-Loading and Charged Conditions of Stabilizers for Semiconductor Microcrystalline Photocatalysts on Photoreduction of Carbon Dioxide

3-1   Introduction

In chapter 2, it was found that the quantum efficiency for the photoreduction of CO_2 increased with decreasing the particle size of the ZnS and TiO_2 microcrystals. To achieve further improvements of the quantum efficiency for the photoreduction of CO_2 was the primary purpose of the present study. The most popular technique to enhance the photocatalytic activities is the loading of electrocatalysts on the semiconductor photocatalysts. Many examples have shown the utility of this approach: For example, photodecomposition of water on TiO_2 and $SrTiO_3$,[32b,64,65] photosynthesis of amino acid on TiO_2 and CdS,[32b,66,67] and photodecomposition of saturated carboxylic acids on TiO_2[32b,68] are greatly enhanced by several kinds of noble metal loadings. In this study, we have tested the loading of several kinds of metals on ZnS microcrystal photocatalysts and found that the loading of Cd was effective in enhancing the quantum efficiency for the photoproduction of formate. It has been reported that ZnS/CdS cocolloids prepared on alumina, clay and Nafion supports showed remarkable photocatalytic activities for hydrogen evolution from aqueous sulfite solutions without loading noble metal electrocatalysts.[69] By combining the effectiveness of the Cd-loading with the reported results on the use of ZnS/CdS colloids, the reduction of CO_2 on solid solutions of ZnS/CdS microcrystals which show sensitivities to visible lights has been investigated.

In cases of using such small semiconductor particles as to show size quantization effects as photocatalysts, the use of stabilizers are required to

prevent agglomeration of the particles though a case of not using the stabilizer was reported.[70] So far, various stabilizers have been used, but only a limited number of studies have investigated the effect of the structure[46] and the charges[33d] of the stabilizers on the activities as photocatalysts of the size quantized particles. It has already been reported[71] that the stabilizers influence the rate of photo-induced reactions on the size quantized particles, but no publication is available for the role of the stabilizers which might change the photo-induced reaction routes. In the present study investigations were made to clarify the effect of the charged conditions of the stabilizers on the photoreduction products of CO_2.

3-2 Experimental

Chemicals

Cadmium perchlorate and lead perchlorate (Kishida), nickel perchlorate, silver perchlorate, copper perchlorate, poly(sodium vinylsulfonate) (averaged MW =1100), polybrene(MW=22500), poly(sodium 4-stylenesulfonate) (MW= 70000) (Aldrich), polyacrylic acid (molecular weight (MW)=150000), polyethyleneimine (MW=70000) (Wako Pure) and poly(allylamine hydrochloride) (MW=70000) (Toyobo) were used as received.

Procedure

The ZnS microcrystalline colloids were prepared by mixing 0.6mM $Zn(ClO_4)_2$ and 0.4 mM Na_2S in an equal volume in the presence of a fine SiO_2 powder having the specific surface area of 200 m^2 g^{-1} which was used as a stabilizer. Details of the preparation procedures were reported in chapter 2. The resulting ZnS colloids contained excess Zn^{2+} ions of 0.1 mM Zn^{2+}. ZnS/CdS microcrystalline solid solution colloids given by the chemical

formula of $Cd_xZn_{1-x}S$ ($0 \leqq x \leqq 1$) were prepared in a similar method to that described above. By fixing the sum of the concentration of $Zn(ClO_4)_2$ and $Cd(ClO_4)_2$ to 0.6 mM, and by adding 0.4 mM Na_2S to the mixed solution of $Zn(ClO_4)_2$ and $Cd(ClO_4)_2$ with an equal volume, 0.2 mM $Cd_xZn_{1-x}S$ microcrystalline colloids were produced in which either Zn^{2+} or Cd^{2+} ions or both were excess, whose total concentration was 0.1 mM. The colloid was aged for 1 day prior to use in photoreduction experiments of CO_2. Bulk ZnS and $Cd_xZn_{1-x}S$ colloids were also prepared using the similar procedures without using the SiO_2 powder as the stabilizing agent. The average size of the ZnS microcrystals was 3.9 nm and that of the bulk ZnS colloids was 45 nm, as determined by a Photal DLS-70 Ar dynamic light scattering apparatus (Otsuka Electronics). The mean particle diameter of the prepared $Cd_xZn_{1-x}S$ microcrystals evaluated from TEM photographs was about 4 nm for all cases independent of x values. On the other hand, the mean particle diameter of the bulk $Cd_xZn_{1-x}S$ was 50 nm for x=0.83 and 0.75, 60 nm for x=0.50 and 0.33, and 80 nm for x=0.

The metal loading of the ZnS particles was carried out in the following way. 3.9 cm^3 of the prepared ZnS colloids (0.78 μmol of ZnS) were put in a quartz cell ($1 \times 1 \times 4.5$ cm^3) having a side branch. 0.1 cm^3 of either one of $Cd(ClO_4)_2$, $Pb(ClO_4)_2$, $Ni(ClO_4)_2$, $AgClO_4$ and $Cu(ClO_4)_2$ of various concentration was added to the ZnS colloids. Finally, 2-propanol was added as a hole scavenger to give its concentration of 1 M, followed by flushing the resulting solution with Ar for 30 minutes to purge off dissolved oxygen. The photodeposition of metals onto the ZnS microcrystals was then attempted by illuminating the prepared reaction solution with a 500 W high-pressure Hg arc lamp through 0.1 M NaI solution to cut off UV lights of wavelengths shorter than ca. 270 nm.

CdS microcrystals were prepared under nitrogen atmosphere by mixing

in an equal volume of 0.4 mM sodium sulfide and 0.6 mM $Cd(ClO_4)_2$ containing a stabilizer of 0.8 mM concentration of monomer unit . Polyacrylic acid, poly(sodium vinylsulfonate) and poly(sodium 4-stylenesulfonate) were used as anionic stabilizers, and poly(allylamine hydrochloride), polyethyleneimine and polybrene were used as cationic stabilizers. The CdS microcrystals with these stabilizers were stable at least for 3 weeks.

The photoreduction of CO_2 was carried out using a quartz cell ($1 \times 1 \times 4.5$ cm^3) having a side branch. 4 cm^3 of the ZnS microcrystals, bulk ZnS suspensions, various metal-loaded ZnS microcrystals, $Cd_xZn_{1-x}S$ microcrystals and CdS microcrystals were put in the cell. In the case of CdS microcrystals 0.1 cm^3 of 0.16 M stabilizer on the monomer basis and 0.32 cm^3 of 2-propanol were added. The pH of the solution was adjusted to 5.5 by addition of appropriate amounts of $NaHCO_3$, followed by bubbling of CO_2 for 20 min. The 500 W high pressure Hg arc lamp was used as a light source for the ZnS microcrystals, bulk ZnS suspensions, the metal-loaded ZnS microcrystals and $Cd_xZn_{1-x}S$ microcrystals, and lights from the lamp were passed through a 0.1 M NaI solution, while the 500 W Xe arc lamp were passed through UV-33 cut off filter (Toshiba) for the CdS microcrystals. The photoreduction experiments were carried out in a water bath at room temperature under magnetically stirring the solution.

Absorption spectra were measured by using a HP8452A diode-array spectrophotometer. The fluorescence spectra were measured with excitation wavelength at 280 nm using a F-3010 fluorescence spectrometer (Hitachi).

The charged conditions of the stabilizers in solution was evaluated using the well-established technique of potentiometric titration.[72] 0.01 M NaOH aqueous solution containing various stabilizers whose monomer concentration was 0.01 M was titrated with 0.01 M $HClO_4$. If acid-base equilibrium is

49

represented by the following equation for anionic and cationic stabilizers, respectively,

$$R^- + H^+ = RH \qquad\qquad RH + H^+ = RH_2^+ \qquad\qquad (22)$$
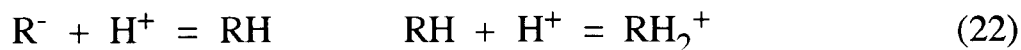
then the fraction of the negative charges (N) and positive charges (P) of the stabilizers is given by

$$N = \frac{[R^-]}{[R^-] + [RH]} \qquad\qquad P = \frac{[RH_2^+]}{[RH] + [RH_2^+]} \qquad\qquad (23)$$

where $[R^-]$, $[RH]$, and $[RH_2^+]$ show the concentration of the respective species on the monomer basis.

Determination of Products

Products in the gas phase were determined by gas chromatography and those in a liquid phase were gas chromatography and high-pressure liquid chromatography, as described in chapter 2. In addition, the quantum efficiency for the photoreduction of CO_2 was determined at 280 nm in the same way as chapter 2.

3-3 Results and Discussion

3-3-1 Quantum Efficiency for Photoreduction of Carbon Dioxide Using Various Metal-loaded Zinc Sulfide Microcrystals

The prepared ZnS microcrystals showed the absorption spectra having an onset wavelength near 315 nm. Fluorescence spectra showed its peak at around 435 nm, which is attributed to the recombination of photogenerated electrons and holes at anion vacancies.[73]

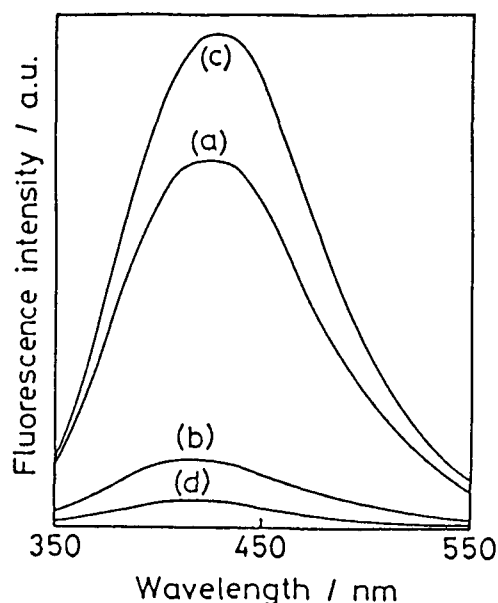Figure 25 shows changes of the fluorescence spectra of 0.2 mM ZnS

Fig. 25. Fluorescence spectra of the ZnS microcrystals. (a) original
ZnS microcrystals before addition of cadmium ions, (b) after addition
of cadmium ions, (c) after subsequent illumination for 30 minutes with
a 500 W Hg arc lamp, and (d) then after introduction of CO_2 for 30
minutes.

microcrystalline colloids caused by the Cd-loading. As described in
experimental section, the ZnS microcrystalline colloids contained 0.1 mM
Zn^{2+} ions. By addition of 5 µM Cd^{2+} ions, the fluorescence intensity of the
colloids was remarkably decreased, suggesting that Cd^{2+} ions worked as a
quencher, but the wavelength of the fluorescence peak was not changed. On
the other hand, the excess Zn^{2+} ions did not work as a quencher.[74] The
inactivity of Zn^{2+} ions for the fluorescence quenching may be related to their
low reducibilities on photoexcited ZnS microcrystals in the presence of 2-
propanol. After 30 minutes-illumination of 4 cm^3 of the ZnS colloids in the
presence and absence of 5 µM Cd^{2+} ions, 0.2 ml of 10 mM MV^{2+} was added
to the colloids, and the amount of resulting $MV^{+\cdot}$ was determined. By
assuming that $MV^{+\cdot}$ was produced by the reaction with the deposited metals

alone, it was found that all Cd^{2+} ions present in the ZnS colloids before illumination were photodeposited, while only 5 % of the Zn^{2+} ions were deposited by the illumination for 30 minutes. The easy electron transfer from ZnS microcrystals to Cd^{2+} was reported by Henglein et al.[74] The results obtained here indicate that Zn^{2+} ions have very weak electronic interaction with the ZnS microcrystals.

When the Cd deposition onto ZnS microcrystals completed, ZnS microcrystals recovered abilities for fluorescence emission, as shown by spectrum(c) of Fig. 25. If CO_2 was introduced at that stage, the fluorescence intensity was decreased again to give spectrum(d) of Fig. 25. The fluorescence intensity in this case was lower than that obtained at the naked ZnS microcrystals in the presence of CO_2, suggesting that photogenerated electrons were more easily scavenged by CO_2 with the Cd-loading. It was found that the pH of the colloids was dropped from 9.0 to 5.5 by the introduction of CO_2, and the pH decrease of this magnitude caused about 75 % decrease in the fluorescence intensity of Cd-loaded ZnS even if CO_2 was absent. Accordingly, the decrease in the fluorescence intensity caused by CO_2 introduction must result from both pH change and quenching action of CO_2.

Figure 26 shows the time course of the production of formate and hydrogen as the reduction products and acetone as an oxidation product for the photoreduction of CO_2 in the presence of 1 M 2-propanol at the Cd-loaded ZnS microcrystals. No other reduction products of CO_2 than formate were detected, as in the case of using naked ZnS microcrystals as a photocatalyst. The amount of oxidation and reduction products satisfied the chemical stoichiometry of the light-induced reactions. Since the production of these substances occurred in proportion to the illumination time, the activity of the ZnS microcrystals was not significantly lost for the time interval given in the figure, suggesting that the deposited Cd on ZnS microcrystals was stable, being
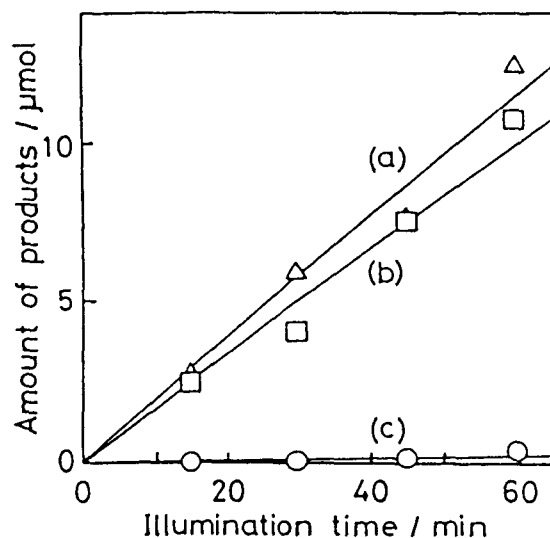
52

Fig. 26. Time course of the production of (a) acetone, (b) formate, and (c) hydrogen on Cd-loaded ZnS microcrystals. Mole ratio of Cd to ZnS microcrystals was 0.025. Other reaction conditions are given in the text.

different from colloidal Cd.[75] The Cd-loaded ZnS microcrystals did not show any appreciable activities in the dark.

Figure 27 shows the quantum efficiency for the photoproduction of each product as a function of the mole ratio of the loaded Cd to the ZnS microcrystals. In all cases it was pre-illuminated for 30 minutes before the CO_2 reduction experiments were performed. As this figure shows, the quantum efficiency for photoproduction of formate was enhanced by Cd-loading of the ZnS microcrystals up to twice as large as that obtained at the naked ZnS microcrystals. The highest quantum efficiency of 42 % was achieved with the Cd-loading of 0.025 mol%. If the fluorescence intensity was measured in the presence of CO_2 before its photoreduction experiments were performed, the intensity was found to decrease with increase in the Cd-loading as shown by a dashed curve in Fig. 27, suggesting that CO_2 makes an electronic interaction with the deposited Cd on ZnS. The quantum efficiency
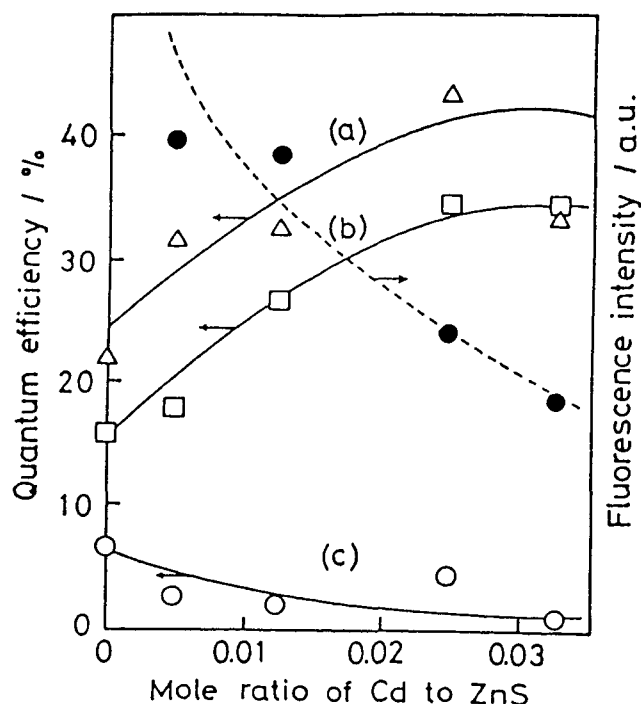
53

Fig. 27. Quantum efficiency for photoproduction of (a) acetone, (b) formate, and (c) hydrogen, and the fluorescence intensity at 435 nm after introduction of CO_2 as a function of the mole ratio of loaded cadmium on the ZnS microcrystals. Illumination time was 30 min.

for the formate production was saturated for the loading over 0.025 mol%. The saturation of the photocatalytic activity with the increase of the loading of metals has been discussed for photoreduction of water using Pt-loaded TiO_2 and CdS powders as photocatalysts in terms of a screening effect of the deposited metals for light absorption in photocatalysts .[76-78] In addition, it may be thought as an another reason that the size of the deposited Cd metal may increase with the increase of the loading of Cd.[79]

It may be speculated that the photo-induced reduction of CO_2 molecules at Cd-loaded ZnS microcrystals takes place with consumptions of photogenerated electrons not only through the conduction bandedge, but also through surface states associated with anion vacancies.[70] The finding that the fluorescence peaked at 435 nm for both naked and Cd-loaded ZnS microcrystals, and that

the absorption onset wavelength was the same and 315 nm between the two kinds of photocatalysts suggests that the anion vacancies locate at 1.07 V more positive than the conduction bandedge. Since CO_2 quenched the fluorescence intensity as described above, the anion vacancies seem to be involved in the photoreduction of CO_2. However, there may be another possibility that the fluorescence quenching occurs even if photogenerated electrons in the conduction band move directly to the deposited metal at which the reduction of CO_2 takes place. In this regard, the involvement of the conduction band process is not ruled out.

Table 2 summarizes the quantum efficiencies for the production of formate, hydrogen and acetone determined at 280 nm for ZnS microcrystals having several kinds of loaded metals. In the preparation of the metal-loaded photocatalysts, 5 μM metal ions were added to the 0.2 mM ZnS

Table 2. Quantum efficiencies for reduction and oxidation products obtained in the photoreduction of CO_2 in the presence of 2-propanol on the ZnS microcrystals having various loaded metals[*1)]

Photocatalyst[*2)]	Quantum efficiency / %		
	HCOO⁻	H_2	$(CH_3)_2CO$
bulk ZnS[*3)]	0	15.1	24.5
Zn / ZnS	15.2	7.3	21.7
Cd / ZnS	32.5	5.0	42.0
Pb / ZnS	13.9	2.8	20.8
Ni / ZnS	10.0	8.4	17.0
Ag / ZnS	10.7	3.4	16.4
Cu / ZnS	4.9	1.7	8.3

[*1)] Metal-loading was made by illumination for 30 minutes.
[*2)] Experiments were carried out in the presence of 0.1 mM Zn^{2+}.
[*3)] Bulk ZnS prepared in the absence of silica. Particle size was 45 nm.

microcrystalline colloids in the presence of 0.1 mM Zn^{2+} for all cases. As already described above for the deposition of Cd, the metal deposition seems to be completed with illumination for 30 minutes except for the Zn deposition where only 5% of the Zn^{2+} ions present in the solution were deposited. It may be speculated that when the metal ions were added, the replacement deposition occurred on the ZnS microcrystal surfaces even without assistance of irradiation, because the solubility products of sulfides of the added metal ions are smaller than ZnS. However, the fluorescence spectrum of the ZnS microcrystalline colloids were not changed by the addition of metal ions. This finding suggests that the formation of the new metal sulfide by the replacement reaction, if any, does not play any significant role in fluorescence of the ZnS microcrystals.

All the loaded metals investigated in the present study gave formate alone. Interestingly, the bulk ZnS did not show any noticeable activity for photoreduction of CO_2. Furthermore, it was found that the loading of the metals tested in the present study except for Cd caused a decrease in the activity for photoreduction of CO_2. No appreciable fluorescence quenching was seen with introduction of CO_2 for Ag, Ni, and Cu-loaded ZnS microcrystals, while the fluorescence quenching was seen for Pb-loaded ZnS microcrystals, as in the case of Cd-loaded ZnS microcrystals. However, the Pb-loaded ZnS showed null activities for CO_2 reduction as shown in Table 2. Presumably, the adsorbed CO_2 on the loaded Pb have a strong interaction with photogenerated electrons in the ZnS microcrystals, but it is not easily reduced due probably to high overvoltage of Pb for the reduction of CO_2.[80,81]

3-3-2 Photoreduction of Carbon Dioxide Using Zinc Sulfide / Cadmium Sulfide Solid Solution Microcrystals

Absorption spectra of $Cd_xZn_{1-x}S$ microcrystals shown in Fig. 28 did not show characteristic absorption of CdS and ZnS, suggesting that CdS and ZnS made solid solutions. With increasing the content of CdS, red-shifts in the absorption spectra are seen. The fluorescence spectra of $Cd_xZn_{1-x}S$ microcrystals also showed one fluorescence peak irrespective of the mole fractions of CdS and its peak was red-shifted with increase of the mole fraction of CdS.

It is well-known that both ZnS and CdS are semiconductors of direct bandgap transition. If it is assumed that $Cd_xZn_{1-x}S$ microcrystals prepared in this work are semiconductors belonging to this class, the bandgap energy of each $Cd_xZn_{1-x}S$ microcrystal can be evaluated by making plots of $(\alpha h v)^2$ vs. hv, as shown in eq. (20). The bandgap energy of various $Cd_xZn_{1-x}S$ microcrystals and the bulk $Cd_xZn_{1-x}S$ powders determined in this way is
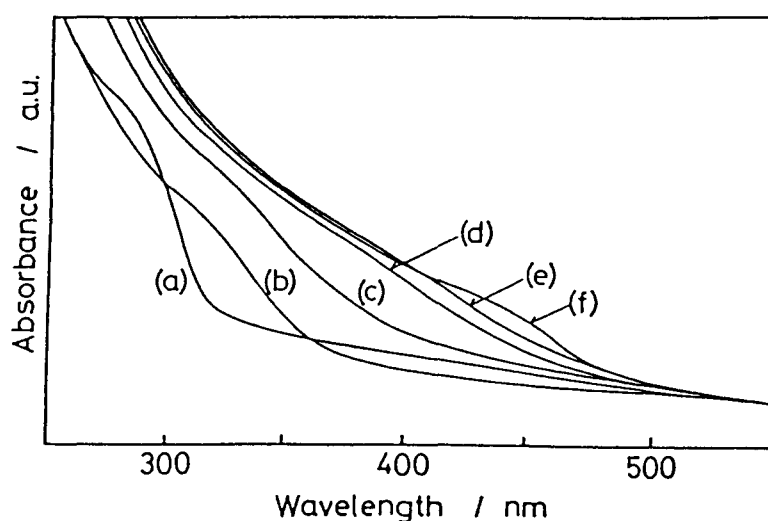

Fig. 28. Absorption spectra of $Cd_xZn_{1-x}S$ microcrystals with (a) x=0, (b) x=0.17, (c) x=0.25, (d) x=0.50, (e) x=0.67, (f) x=1.0.

shown in Fig. 29 as a function of the mole fraction of CdS. The bandgap energy of the microcrystals is larger than that of the bulk powders if comparison is made for the same composition.

Figure 30 shows the time course for the production of formate and hydrogen as reduction products and acetone as an oxidation product when the $Cd_{0.5}Zn_{0.5}S$ microcrystals were used as the photocatalyst. It is noticed that the reduction products were produced after 8 minutes illumination, while acetone was produced without the time lags. The time lags did not appear in the use of ZnS microcrystals, but at $Cd_xZn_{1-x}S$ it increased with increase in the mole fraction of CdS. After the appearance of the time lags $Cd_xZn_{1-x}S$ microcrystals changed their color from transparent yellow to dark brown, which returned to original yellow by exposing to the air, suggesting that the reduction of Cd^{2+} ions to give highly active Cd metals took place preferentially in the beginning of the illumination. As described in experimental section, excess Cd^{2+} ions were present in the $Cd_xZn_{1-x}S$ colloids,

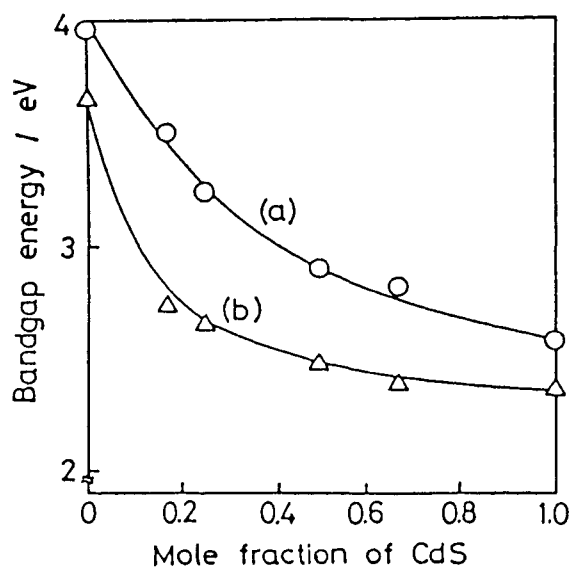Fig. 29. Bandgap energy of (a) $Cd_xZn_{1-x}S$ microcrystals and (b) bulk $Cd_xZn_{1-x}S$ powders as a function of mole fraction of CdS.
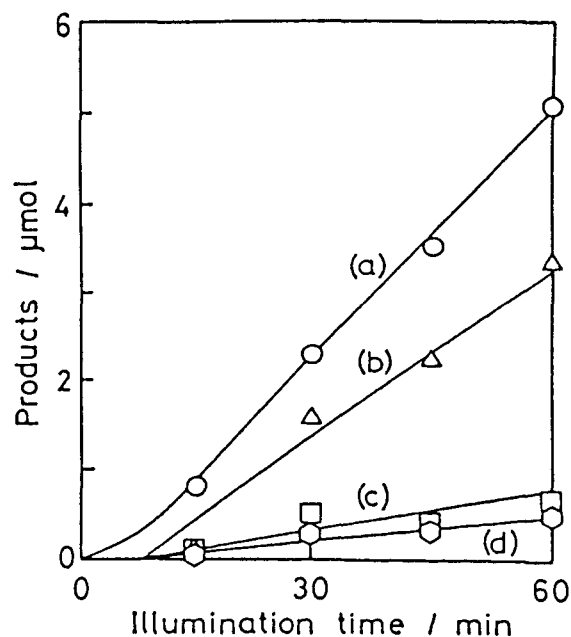
Fig. 30. Time course of the production of (a) acetone, (b) hydrogen, (c) CO, and (d) formate on $Cd_{0.5}Zn_{0.5}S$ microcrystals. Other reaction conditions are given in the text.

depending on the composition. If it is assumed that the mole ratio of the excess Cd^{2+} ions to the Zn^{2+} ions is equal to that of the preparation solutions of $Cd_xZn_{1-x}S$ before the addition of S^{2-}, the number of moles of the excess Cd^{2+} ions present in the cell is greater with increasing the mole fraction of CdS; it is 0.067, 0.10, 0.20, 0.27 and 0.40 μmol for the CdS mole fraction of 0.17, 0.25, 0.50, 0.67 and 1.0, respectively. The finding that the time lags required for the reduction products (formate, CO, and H_2) to be produced became long with an increase in the mole fraction of CdS in $Cd_xZn_{1-x}S$, then suggests that the deposition of Cd^{2+} ions took place preferentially in the time lags.

The production rates of formate, CO and hydrogen on the $Cd_xZn_{1-x}S$ microcrystals were determined from the linear dependence of their productions on the illumination time, and the results are shown in Fig. 31 as a function of the mole fraction of CdS. With increasing the mole fraction of
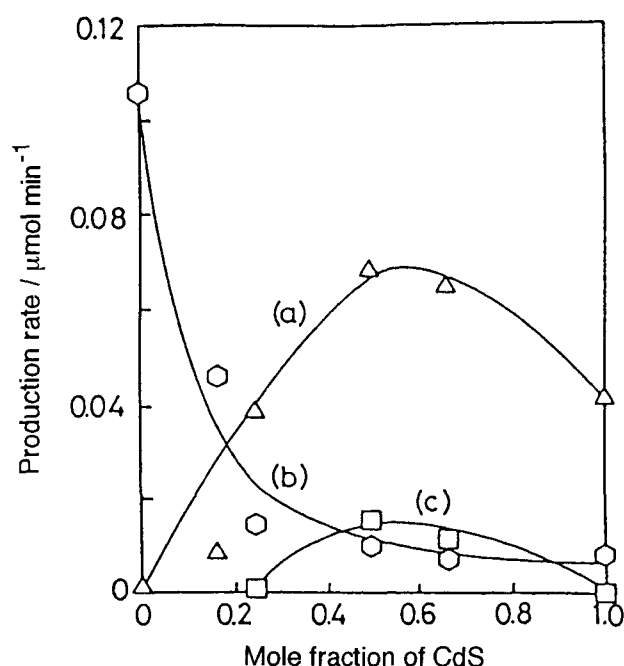
Fig. 31. Production rate of (a) hydrogen, (b) formate and (c) CO on
$Cd_xZn_{1-x}S$ microcrystals.

CdS the rate of formate production decreased, while the hydrogen evolution became predominant. In a range of the mole fraction of CdS between 0.5 and 0.67, CO was produced as a minor reduction product of CO_2. As shown in Fig. 27, the deposited Cd enhanced the photocatalytic activity for the CO_2 reduction to formate without producing CO. If this fact is taken into consideration, it is not easily expected to have CO as the reduction products for $Cd_xZn_{1-x}S$.

The intensity of fluorescence peak of 0.2 mM $Cd_xZn_{1-x}S$ colloids which appeared in wavelengths between 435 - 570 nm depending on the value of x was quenched by introduction of CO_2. It was found that the degree of the fluorescence quenching was varied with the value of x and remarkable quenching was seen for $Cd_xZn_{1-x}S$ microcrystals having x= 0.5 to 0.67, at which CO production from CO_2 was seen. However, the fluorescence quenching observed there was in perfect accord with that observed with

60

variation of pH of the colloids, suggesting that the fluorescence quenching is solely related to adsorption of H^+ ions. Then it is speculated that adsorbed H^+ ions plays a key role in determining reduction behaviors of CO_2.

3-3-3 Effect of Charged Conditions of Stabilizers for Cadmium Sulfide Microcrystalline Photocatalysts on Photoreduction of Carbon Dioxide

Figure 32 shows the degree of charging for polyacrylic acid and polyethyleneimine determined from eq. (23) as a function of pH. From each curve of this figure, the degree of charging of polyacrylic acid and polyethyleneimine at pH 5.5, at which the photoreduction experiments of CO_2 were carried out, was 0.30 and 0.50, respectively. The degree of charging at pH 5.5 for the other stabilizers was evaluated in the same way. The degree of negatively charging was 0.97 and 1.0 for poly(sodium vinylsulfonate) and
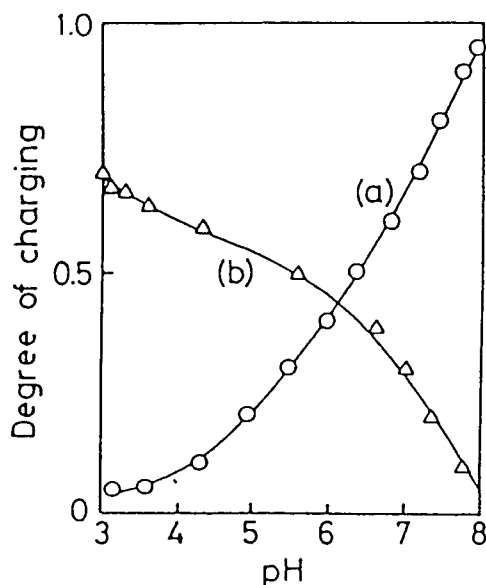

Fig. 32. Degree of charging of (a) polyacrylic acid and (b) polyethyleneimine as a function of pH.

poly(sodium 4-stylenesulfonate), respectively, while the degree of positively charging was 0.98 and 1.0 for poly (allylamine hydrochloride) and polybrene, respectively.

Absorption spectra of CdS microcrystals in the presence of polyacrylic acid and polyethyleneimine are shown in Fig. 33. Both spectra gave the absorption onset at wavelengths much shorter than ca. 520 nm which is valid for the bulk CdS particles, suggesting that the quantized microcrystals were prepared. Judging from a theoretically derived relation between the particle diameter and the bandgap,[82] CdS microcrystals prepared here were less than 5 nm in the diameter. If the bandgap (E_g) of CdS microcrystals in the prepared colloids were evaluated by applying their absorption spectra to $(\sigma h v)^2$ vs. hv relation shown in eq. (20), results given in Table 3 were obtained.
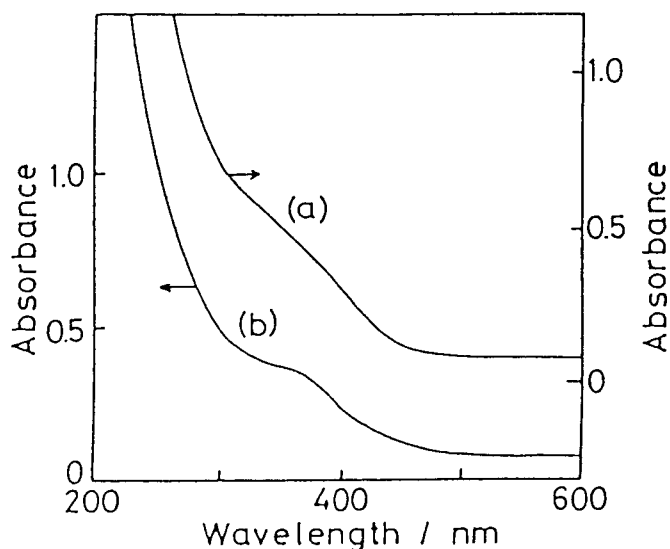

Fig. 33. Absorption spectra of CdS microcrystals stabilized by (a) polyacrylic acid and (b) polyethyleneimine. [CdS]=0.2 mM.

Figure 34 shows the time course of the production of reduction and oxidation products for CO_2-saturated solution containing 1 M 2-propanol in the presence of polyacrylic acid and polyethyleneimine. As this figure shows, formate was obtained as a major product of the CO_2 photoreduction when polyacrylic acid was used as the stabilizer, while CO was obtained with the use of polyethyleneimine. In both cases, hydrogen was evolved as another reduction product and acetone was a sole oxidation product. Blank experiments confirmed that no reaction took place in the absence of CO_2 and 2-propanol. Absorption spectra of the CdS microcrystals were unchanged with illumination for 6h. These results suggest that the production of oxidation products and reduction products occurred with high chemical stoichiometry. Table 3 summarizes photoreduction experiments of CO_2 obtained using various stabilizers adopted in this study. The results shown in
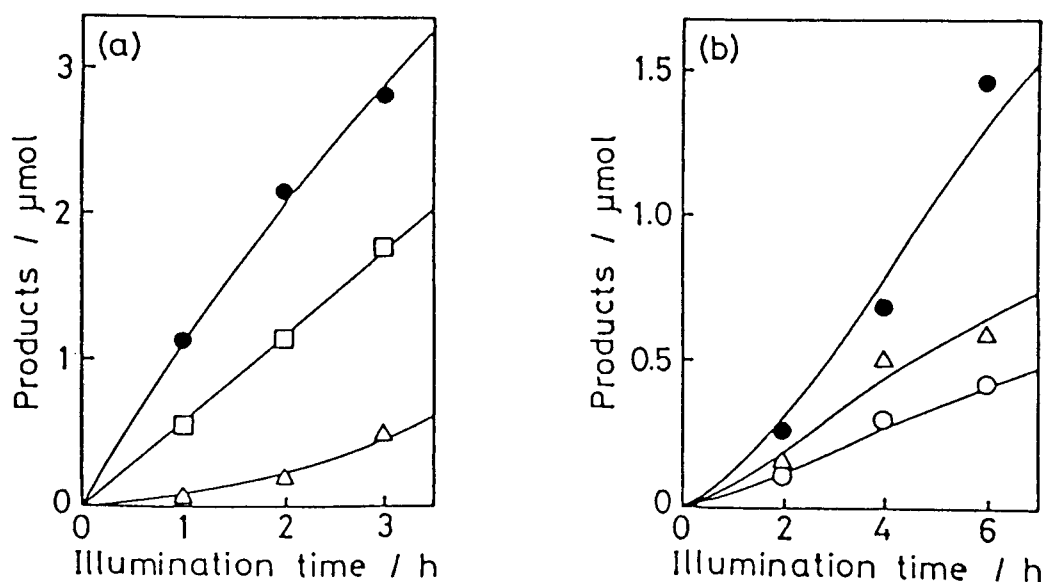

Fig. 34. Time course of the production of (□) formate, (○) CO, (△) hydrogen and (●) acetone using 0.2 mM CdS microcrystals containing 1 M 2-propanol in the presence of 4 mM (a) polyacrylic acid and (b) polyethyleneimine on the monomer basis.

Table 3. Results of photoreduction of CO_2 using CdS microcrystals
stabilized by various polymers.

Stabilizer	E_g/eV	Illumination time / h	Product / μmol		
			HCOO⁻	CO	H_2
poly(sodium vinylsulfonate)	2.68	4	0.73	0	0.090
poly(sodium 4-stylenesulfonate)	2.66	4	0.88	0	0.046
polyacrylic acid	2.80	3	1.77	0	0.59
poly(allylamine hydrochloride)	2.80	16	0	0.75	0
polybrene	2.71	9	0	0.11	0
polyethyleneimine	2.85	6	0	0.40	0.72
polyethyleneimine[*1]	2.48	15	0	0.15	0.32

[*1] Prepared CdS microcrystal was stood for one month before the
photoreduction of CO_2.

this table suggest that the use of negatively charged stabilizers such as
poly(sodium vinylsulfonate), poly(sodium 4-stylenesulfonate) favored the
production of formate, while the use of positively charged stabilizers such as
polyallylamine and polybrene were effective in selective production of CO
from CO_2. The CdS microcrystals stabilized by polyethyleneimine became
large with storage at room temperature for one month, and the activities as the
photocatalyst decreased, but the reduction products obtained were unchanged,
as shown also in the table.   The effect of charging of the stabilizers on the
relative production rate of the reduction products of CO_2 to hydrogen was
investigated by changing the pH of the solution for cases of using polyacrylic
acid and polyethyleneimine, and the results obtained are shown in Fig. 35.
Though the magnitude of the relative rates was different between the two
kinds of stabilizers used, an increase in the amount of charges of the stabilizers
favored the reduction of CO_2 either to formate or to CO.

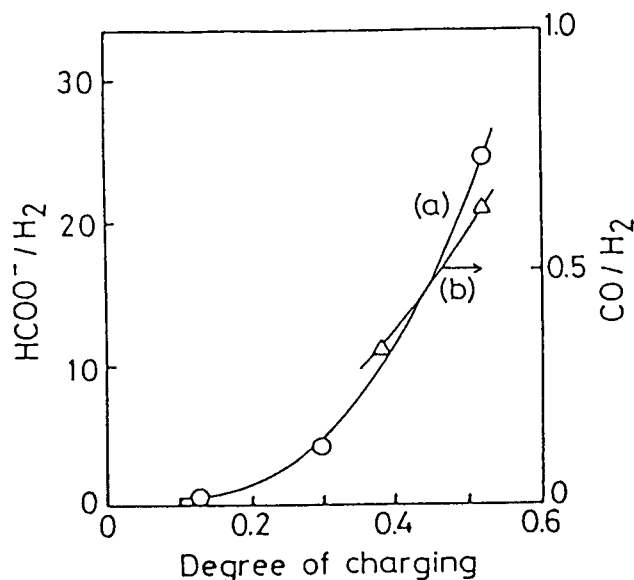The photoreduction of CO_2 is initiated by one-electron reduction of

Fig. 35. Ratio of the amount of formate to hydrogen produced (a) and
that of CO to hydrogen produced (b) as a function of degree of charging
of (a) polyacrylic acid and (b) polyethyleneimine.

adsorbed CO_2 to give CO_2^-. When the photocatalyst is surrounded by
negatively charged stabilizers, the resulting CO_2^- can make adsorption onto
the photocatalyst surfaces with the carbon atom of CO_2^-, resulting in the end-
on type adsorption. In contrast, in cases where the photocatalyst is covered
with positively charged stabilizers, the adsorption of CO_2^- can occur with
involvement of both the carbon atom and negatively charged oxygen atom of
CO_2^-, resulting in the so-called side-on adsorption. The end-on type
adsorption favors the formate production, while the side-on type the carbon
monoxide production.[83] The difference in the rate of production between
formate and CO may result from differences in the stability of adsorbed CO_2
in these two different configurations.

3-4 Summary

The product of CO_2 photoreduction at ZnS microcrystals loaded by metals such as Cd, Pb, Ni, Ag and Cu was formate and the loading of Cd increased the quantum efficiency for the photoproduction of formate up to 32.5%, which was twice as large as that obtained on the naked ZnS microcrystals. Solid solutions of ZnS/CdS microcrystals, however, did not exhibit high activities for photoreduction of CO_2. The use of stabilizers having negative charges such as polyacrylic acid for CdS microcrystals in aqueous solutions yielded selectively formate as a photoreduction product of CO_2, while positively charged stabilizers such as polyethyleneimine worked well for selective production of CO. Furthermore, it was found that the rate of photo-induced reduction of carbon dioxide was influenced by the amount of charges of the stabilizers used.

Chapter 4 Photo-Induced Electron Transfer from Zinc Sulfide Microcrystals Modified with Various Alkanethiols to Methyl Viologen

4-1 Introduction

Semiconductor microcrystals showing the size quantization effect show high photocatalytic activities for various photoreactions such as photoreductions of CO_2 [17,70] and water[46,84], photo-hydrogenations of alkyne[55] and photo-Kolbe reactions[33] as compared to the corresponding bulk particles. In relations to photocatalysis of semiconductor microcrystals, photo-induced electron transfers have been investigated using reversible redox species such as MV^{2+},[71,85-88] nile blue A,[89a] oxazine 725,[89a] methylene blue,[89a] and phenosafranin.[89b]

The semiconductor microcrystals have been prepared with use of several different techniques. It has been shown for chalcogenide semiconductor microcrystals such as CdS, ZnS, CdSe, ZnSe, and PbS that modification of their surfaces with thiophenol,[90,91] selenophenol,[90,92] pentafluorothiophenol,[92] and 4-hydroxythiophenol[93] provides a useful means for preparation of microcrystals with a narrow size distribution. Furthermore, the surface-modified semiconductor microcrystals, which are denoted as capped semiconductor microcrystals, can be isolated as powders from preparation baths and the obtained powders can be redispersed in organic solvents. If one wants to use the capped semiconductor microcrystals as photocatalysts, it is essential to know the effect of the capping molecules on apparent photocatalytic activities. Effects of surface charges of the capping organic molecules on photoreduction of MV^{2+} were investigated for PbS microcrystals capped with 4-hydroxythiophenol[93a] and 4-aminothiophenol.[93b]

In the present study photo-induced reduction behaviors of MV^{2+} on ZnS microcrystals capped with alkanethiols having different alkyl chain lengths were investigated. With comparative purposes, photoreduction behavior on bulk ZnS particles was also investigated.

4-2   Experimental

Chemicals

Sodium dioctylsulfosuccinate (AOT, Aldrich), ethanethiol, butanethiol, octanethiol, heptane (Wako Pure) and MV^{2+} were used as received. Methanol and acetonitrile (Wako Pure) were distilled prior to use. Commercially available ZnS powders (Nacalai Tesque) having 3 μm diameter and 116 m^2 g^{-1} specific surface area were used as the bulk ZnS particles.

Procedure

The preparation procedure of thiol-capped ZnS microcrystals was followed to that reported by Brus et al.[90] Distilled water was added to heptane containing 0.16 M AOT under agitation in a volume ratio of 0.02, resulting in a homogeneous and transparent reverse-micellar solution with a total volume of 100 cm^3, which was divided into two halves. To one of them 0.16 cm^3 of 1 M $Zn(ClO_4)_2$ aqueous solution was added and to the other 0.16 cm^3 of 1 M Na_2S aqueous solution was added, and they were individually agitated for 30 min. Then these two solutions were mixed under vigorous agitation, resulting in a ZnS-contained reverse-micellar solution. 0.080 cm^3 of 1 M zinc perchlorate aqueous solution was further added to this solution to give the final mole ratio of the added Zn^{2+} to S^{2-} of 1.5. Finally, various alkanethiols were added so as to give 6.77 mM to cap the surface of the ZnS microcrystals. After stirring for 4 h, the solvent of the colloidal solution was

evaporated at room temperature, and an obtained white solid was put in acetonitrile for overnight to remove free alkanethiols contained in the white solid as impurities. After decantation, a small amount of methanol was added and the resulting white suspension was centrifuged to discard the supernatant. The procedure of addition of methanol and centrifuge was repeated until the supernatant did not give any appreciable absorption due to AOT.

The amount of carbon, hydrogen and sulfur included in the alkanethiol-capped ZnS microcrystals was determined by elemental analysis. To determine the amount of zinc contained in the microcrystals, 1 mg of the microcrystals was heated at 400 °C for 2 h in an electric furnace to convert ZnS into ZnO, which was then dissolved by 1 cm^3 of 1 M $HClO_4$ solution. The amount of the resulting Zn^{2+} ions was determined by atomic absorption spectrometry. The particle diameter of the alkanethiol-capped ZnS microcrystals prepared was determined by TEM using a H-9000 transmission electron microscope at operation voltage of 300 kV. The samples were prepared by dropping ZnS microcrystals dispersed in methanol onto a Cu grid, followed by drying in a stream of argon gas. X-ray diffraction analysis was carried out using a XD-3A diffractometer (Shimadzu) and a VG-10R goniometer (Shimadzu). The Cu Kα (λ= 0.1541 nm) line was used in the measurements.

Photo-induced reduction of MV^{2+} was investigated using methanol solution containing 4 mM alkanethiol-capped ZnS microcrystals or 14 mM bulk ZnS particles. The cell used was made of quartz having a side branch and its capacity was 4.5 cm^3. Before measurements, the reaction solution was vigorously bubbled by argon to purge of dissolved oxygen. Illumination was carried out with light of wavelengths longer than 300 nm which were obtained by passing light from a 500 W high-pressure Hg arc lamp through a UV-d36b filter (Toshiba). The light intensity was 30 mW cm^{-2}. The absorption

spectra were measured in one second interval using a HP8452A diode array spectrophotometer. The concentration of $MV^{+\cdot}$ produced was determined from absorbance at 396 nm using the molar extinction coefficient of 42900 $M^{-1}cm^{-1}$.[94] The concentration of formaldehyde produced was determined by a colorimetry using chromotropic acid.[95]

4-3 Theoretical Evaluation of Degree of Capping of ZnS Microcrystals with Modified Thiol Molecules

Zn^{2+} ions and S^{2-} ions that occupy a sphalerite unit cell are shown in Fig.36 where a Zn^{2+} ion is placed at (000). If the length of the unit cell is given by d_0 and unit vectors for x, y and z-direction are given by $\vec{l}$= (100), $\vec{m}$= (010) and $\vec{n}$= (001), the position vector of Zn^{2+} ions ($\vec{Zn}$) of ZnS
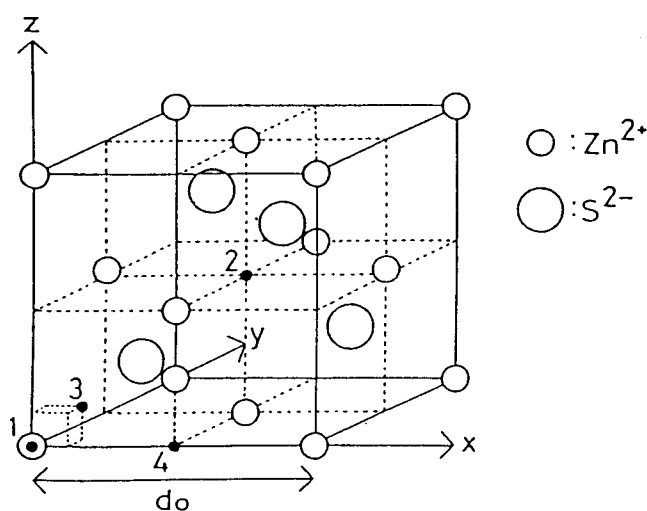

Fig. 36. Crystal structure of sphalerite ZnS. Numbers 1-4 show crystal center.

microcrystals is given by

$$\vec{Zn} = d_0 / 2 \, (\, a\vec{l} + b\vec{m} + c\vec{n} \,) \tag{24}$$

where a, b and c are integers and the sum of a, b and c is even.

If a Zn^{2+} ion is placed at the center, all S^{2-} ions are spatially directed to the corners of a regular tetrahedron, and then the position vectors of four S^{2-} ions surrounding a Zn^{2+} ion are given by eqs. (25)-(28).

$$\vec{S_1} = d_0 / 2 \, (\, a\vec{l} + b\vec{m} + c\vec{n} + (1/2 \; 1/2 \; 1/2) \,) \tag{25}$$

$$\vec{S_2} = d_0 / 2 \, (\, a\vec{l} + b\vec{m} + c\vec{n} + (1/2 \; -1/2 \; -1/2) \,) \tag{26}$$

$$\vec{S_3} = d_0 / 2 \, (\, a\vec{l} + b\vec{m} + c\vec{n} + (-1/2 \; 1/2 \; -1/2) \,) \tag{27}$$

$$\vec{S_4} = d_0 / 2 \, (\, a\vec{l} + b\vec{m} + c\vec{n} + (-1/2 \; -1/2 \; 1/2) \,) \tag{28}$$

If the crystal center of the ZnS microcrystals is chosen as a center of the point symmetry we have four point symmetry centers. These position vectors are given by

$$\vec{A_1} = d_0 / 2 \, (\, 0\vec{l} + 0\vec{m} + 0\vec{n} \,) \tag{29}$$

$$\vec{A_2} = d_0 / 2 \, (\, 1\vec{l} + 1\vec{m} + 1\vec{n} \,) \tag{30}$$

$$\vec{A_3} = d_0 / 2 \, (\, 1/4\vec{l} + 1/4\vec{m} + 1/4\vec{n} \,) \tag{31}$$

$$\vec{A_4} = d_0 / 2 \, (\, 1\vec{l} + 0\vec{m} + 0\vec{n} \,) \tag{32}$$

Then the positions of Zn^{2+} ions and S^{2-} ions in the ZnS microcrystals are respectively given by

$$\vec{Zn} - \vec{A_i} \quad (\, i = 1,2,3,4 \,) \tag{33}$$

$$\vec{S_j} - \vec{A_i} \quad (\, i = 1,2,3,4, \; j = 1,2,3,4 \,) \tag{34}$$

and Zn^{2+} ions and S^{2-} ions included in spherical ZnS microcrystals of the radius of r must satisfy following inequalities.

$$r \geqq \, | \, \vec{Zn} - \vec{A_i} \, | \tag{35}$$

$$r \geqq \, | \, \vec{S_j} - \vec{A_i} \, | \tag{36}$$

The sum of Zn^{2+} and S^{2-} ions determined by this simulation was very close to that obtained by simple calculation based on the density of the sphalerite

71

ZnS and the number of Zn^{2+} and S^{2-} ions per unit cell (4 for both Zn^{2+} and S^{2-}), as shown in Fig. 37. The outermost Zn^{2+} and S^{2-} ions which satisfy eq. (35) and eq. (36) are denoted as Surface-Zn and Surface-S, respectively, as shown in Fig. 38. Surface-Zn and -S can form, respectively, bonds with S^{2-} and Zn^{2+} ions outside a ZnS particle which are denoted as Outer-S and Outer-Zn, respectively (see Fig. 38). Table 4 shows the results of the calculation of the sum of Zn^{2+} and S^{2-} ions which are present inside spherical ZnS microcrystals, Surface-Zn and -S, and Outer-Zn and -S of naked ZnS microcrystals having various particle sizes. The values given in this table show averages of calculated values for each crystal. The maximum number of thiol molecules contained in the surface capping is evaluated by assuming that the capping with thiol molecules occurs at both Surface-S and Outer-S.
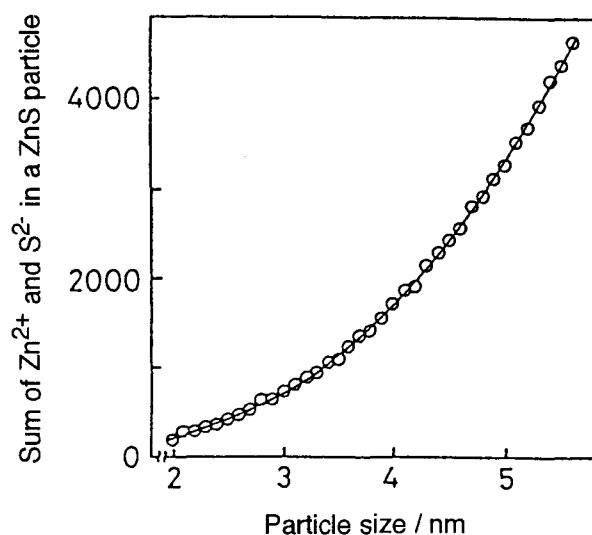

Fig. 37. Sum of Zn^{2+} ions and S^{2-} ions contained in a ZnS particle as a function of particle size: (o) value simulated by the method described in the text. Solid line shows a relation obtained by calculations based on the density of ZnS and the number of Zn^{2+} and S^{2-} ions per unit cell.
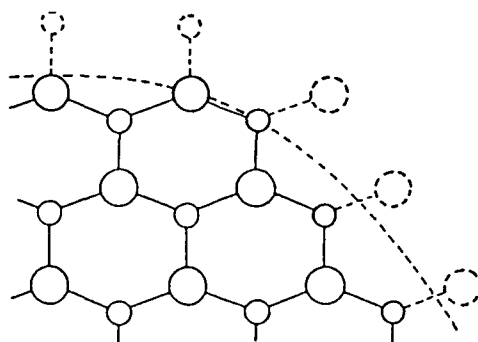
Fig. 38. Partial cross section of a ZnS microcrystal structure. (◯)
Surface-S, (○) Surface-Zn, (◌) Outer-S, and (◌) Outer-Zn.

Table 4. Number of each Zn^{2+} and S^{2-} defined in the text at various
diameters.

Diameter/nm	$Zn^{2+,*1)}$	$S^{2-,*2)}$	Surface-Zn	Surface-S	Outer-Zn	Outer-S
3.6	627	604	192	148	160	216
3.7	675	688	168	184	224	180
3.8	683	736	128	228	276	148
3.9	767	784	176	216	240	208
4.0	887	820	268	156	156	316
4.1	935	928	232	216	234	256
4.2	959	952	232	216	246	256
4.3	1055	1088	216	268	306	228
4.4	1157	1136	270	240	264	312

[*1)] Sum of Zn^{2+} ions which satisfy eq. (35).
[*2)] Sum of S^{2-} ions which satisfy eq. (36).

4-4   Results and Discussion

4-4-1   Characterization of Zinc Sulfide Microcrystals Capped with Various Alkanethiols

Figure 39 shows an absorption spectrum of 2 mM octanethiol-capped ZnS microcrystals dispersed in methanol. The absorption spectrum had a shoulder which is characteristics of exciton absorption.[73] The shoulder was not seen in alkanethiol molecule itself. The absorption spectra of ZnS microcrystals capped with other alkanethiols had similar shapes except for a little blue-shift of the absorption onset. The band gap energy (E_g) of the ZnS microcrystals was determined by applying an onset region of absorption spectrum to $(\alpha h v)^2$ vs. hv plots shown in eq. (20). The determined bandgap values were 3.96 eV for the octanethiol-capping, and 3.94 and 3.96 eV for the capping with ethanethiol and butanethiol, respectively.

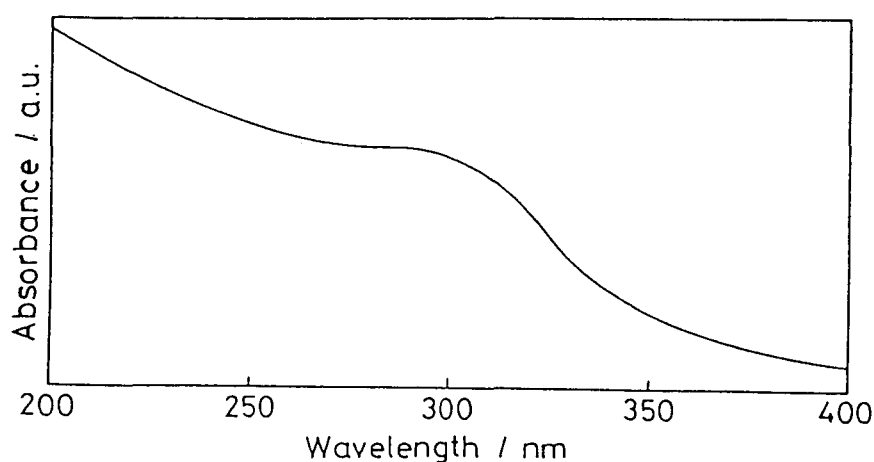Figure 40 shows a TEM photograph of the octanethiol-capped ZnS

Fig. 39. Absorption spectrum of 2 mM octanethiol-capped ZnS microcrystals.
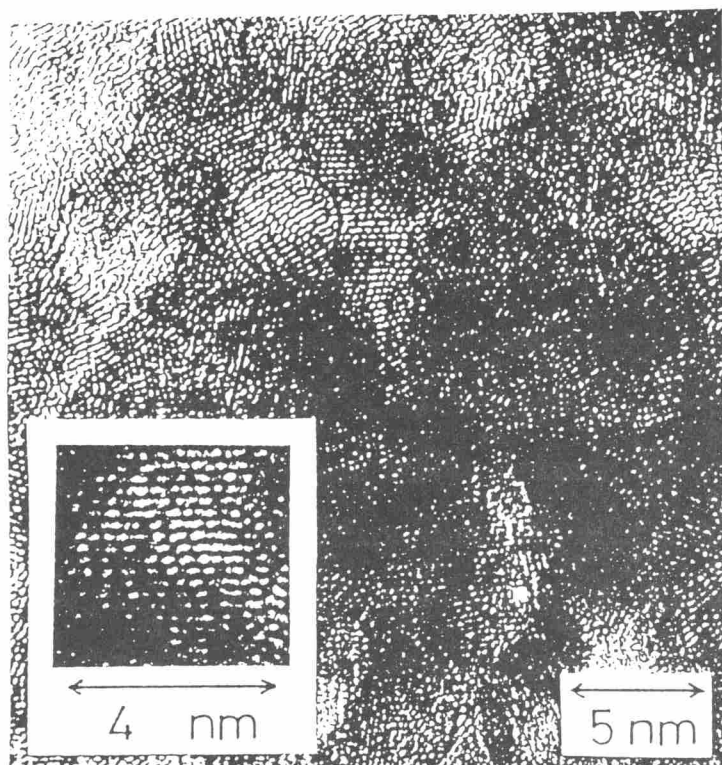
Fig. 40. High resolution TEM images of octanethiol-capped ZnS microcrystals.

microcrystals. Though it is difficult to distinguish each microcrystal because of the overlapping of a lot of lattice stripes, each microcrystal was spherical as will be recognized from the inset of Fig. 40. A lot of lattice planes of 0.31 nm distance are seen, which are consistent with those of a sphalerite ZnS crystal (0.312 nm[96]). Electron diffraction and X-ray diffraction analyses also supported the sphalerite structure of the thiol-capped ZnS microcrystals.

Figure 41 shows a size distribution of the ZnS microcrystals capped with three different alkanethiols, determined from several TEM photographs. The average particle size and the standard deviation were 4.1 nm and 0.6 nm, 3.9 nm and 0.4 nm, and 4.0 nm and 0.5 nm for the ethanethiol, butanethiol and octanethiol-capped ZnS microcrystals, respectively, indicating that the size of
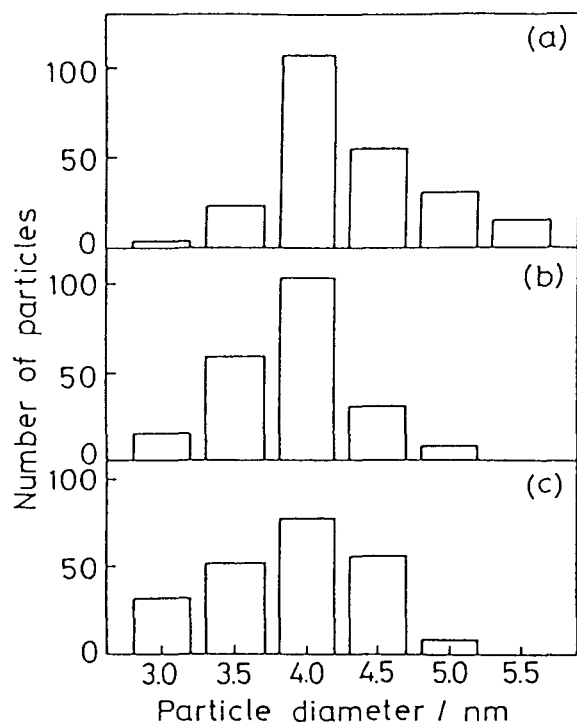
Fig. 41. Size distribution of ZnS microcrystals capped with (a)
ethanethiol, (b) butanethiol, and (c) octanethiol. Size distribution was
obtained for 200 particles.

the ZnS microcrystals was not influenced by the length of alkyl chains of the
capping reagents.

Relations between the particle diameter and the bandgap of the
semiconductor microcrystals have been published by several groups.[82,97-100]
If the above-described bandgap values are applied to the tight-binding
approximation published by Lippens and Lannoo,[82] the particle diameters of
the ZnS microcrystals of 4.1 nm, 4.0 nm and 4.0 nm are obtained for the
ethanethiol, butanethiol and octanethiol capping, respectively, which agree with
values determined by observations with TEM.

To get information on the degree of surface modification with the capping
reagent, the number of Zn^{2+} and S^{2-} ions of the surface of ZnS microcrystals

exposed to the air was first evaluated as a function of the particle size using computer simulation which was successfully applied to evaluation of surface structures of thiophenol-capped PbS microcrystals,[93a] as already described in the preceding section. If it is assumed that the alkanethiol capping takes place at all S atoms and Zn atoms of the microcrystal surfaces (see Fig. 38), the number of capped thiol molecules at full capping can be obtained based on the number of Zn^{2+} and S^{2-} ions of the surfaces of ZnS microcrystals. By taking the experimentally determined size distribution into consideration, mole ratios of Zn, S, C and H of the ZnS microcrystals are calculated for cases of full coverage with three kinds of thiols. The results are shown in Table 5 together with the experimentally obtained ones. It is seen that the calculated values agree well with the experimentally obtained ones in all cases, indicating that all Zn^{2+} and S^{2-} of the ZnS microcrystal surfaces were occupied by the thiol molecules. The full modification with thiols is not unreasonable from the

Table 5. Mole ratio of S, C, and H to Zn estimated in the experiment and theoretical method.

Capping reagent		Zn	S	C	H
ethanethiol	E[*1)]	1	1.2	1.4	3.0
	T[*2)]	1	1.2	1.2	3.1
butanethiol	E	1	1.2	1.9	4.2
	T	1	1.2	1.9	4.3
octanethiol	E	1	1.3	4.4	8.4
	T	1	1.2	4.0	8.6

[*1)] Mole ratio determined by atomic absorption spectrometry and elemental analysis.
[*2)] Mole ratio estimated by calculations using the procedures described in Appendix.

following geometrical considerations. A relative magnitude of the S-S distance of sphalerite ZnS to the diameter of the cross section of the alkyl chain determines whether or not the full modification with thiols can be achieved. The S-S distance is 0.38 nm,[101] while the cross section of the alkyl chain of thiol molecule is 0.185 nm^2 [102] if the surface modification is made perpendicularly to the ZnS microcrystal surface. This gives basis for full capping of ZnS microcrystals with thiol molecules. When thiol molecules are bound to Zn^{2+} ions of the microcrystal surfaces, they contain surface-bound S atoms which are given by dotted circles in Fig. 38, and are also denoted here as Outer-S. Thiol-capped ZnS microcrystals contain S atoms originated from the capped thiol as a constituent of the microcrystals on their surfaces which are denoted as Surface-S (see Fig. 38).

4-4-2   Photo-Induced   Electron   Transfer   from   Alkanethiol-Capped ZnS   Microcrystals   to   Methyl   Viologen

Figure 42 shows the time course of the $MV^{+\cdot}$ production on the ethanethiol-capped ZnS microcrystals for three different concentrations of MV^{2+} in methanol that worked as a hole scavenger as well as the solvent. From the beginning of the illumination, the $MV^{+\cdot}$ production proceeded linearly with the illumination time. The amount of the MV^{2+} consumed after the illumination for 1 min was 5.8 nmol, which was 1.9 % of the amount included in 0.1 mM MV^{2+}, resulting in a negligible influence of the change in the concentration of MV^{2+} on the production rate of $MV^{+\cdot}$ for the time scale of this experiment. The same was true for ZnS microcrystals capped with butanethiol and octanethiol. As shown in Fig. 42, formaldehyde was produced when the reduction of MV^{2+} occurred, and its amount was nearly one half that of $MV^{+\cdot}$, suggesting that following reactions took place.
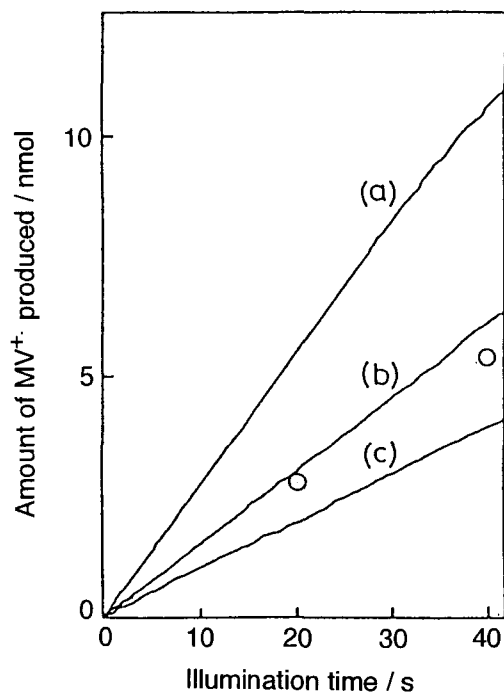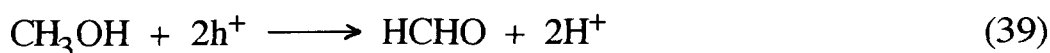
Fig. 42. Time course of $MV^{+\cdot}$ production on 4 mM ethanethiol-capped ZnS microcrystals. Concentration of MV^{2+}:(a) 0.3 mM, (b) 0.2 mM, (c) 0.1 mM. The open circle shows the production amount of formaldehyde in methanol containing 0.3 mM MV^{2+}.

$$h\nu \longrightarrow e^- + h^+ \tag{37}$$

$$2MV^{2+} + 2e^- \longrightarrow 2MV^{+\cdot} \tag{38}$$

$$CH_3OH + 2h^+ \longrightarrow HCHO + 2H^+ \tag{39}$$

Absorption spectra of ethanethiol-capped ZnS microcrystals and infra-red spectra of the capping thiol molecules before and after the photoreduction experiments for 3 min did not change at all, suggesting that the ZnS microcrystals and the capping thiol molecules were not photodegraded in that time period. It is seen in curve (a) of Fig. 42 that the production rate of $MV^{+\cdot}$ becomes a little suppressed with irradiation for longer than ca. 30 s. We believe that the deviation of the time course from linearity results from occurrence of back reaction, that is, reoxidation of the produced $MV^{+\cdot}$.[93b]

Ebbesen and Ferraudi reported[103] that photoreduction of MV^{2+} occurs in pure methanol and aqueous methanol solution under illumination with a N_2 laser or an excimer laser even if no other photosensitizer was available. Blank experiments conducted in the absence of the capped ZnS microcrystals, however, showed that under our experimental conditions no $MV^{+\cdot}$ molecules were produced. The concentration of MV^{2+} used in this chapter was one to three orders of magnitude smaller than that used by Ebbesen and Ferraudi, and the illumination intensity was one thousandth that employed by them. Considering these, it is believed that the photoreaction of MV^{2+} with methanol occurs with illumination under relatively high illumination intensity of MV^{2+} of high concentrations.

The initial rate of the $MV^{+\cdot}$ production was determined from the slope of the time course for three kinds of thiol-capped ZnS microcrystals, and are shown in Fig. 43 as a function of the concentration of MV^{2+}. It is seen that
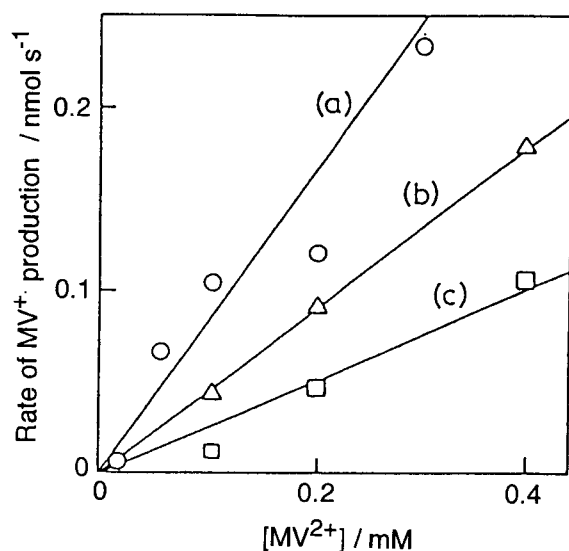

Fig. 43. Rate of $MV^{+\cdot}$ production as a function of the concentration of MV^{2+} for (a) ethanethiol, (b) butanethiol and (c) octanethiol-capped ZnS microcrystals.

the initial rate of the $MV^{+\cdot}$ production increases linearly with an increase in the concentration of MV^{2+}. The rate constant determined from the slope of the plots are 2.23×10^{-4} s^{-1}, 1.17×10^{-4} s^{-1} and 6.7×10^{-5} s^{-1} for the ethanethiol, butanethiol and octanethiol-capped ZnS microcrystals, respectively. The rate constant of the $MV^{+\cdot}$ production becomes high with decreasing the carbon number of the alkanethiols, as shown in Fig. 44. With an increase in the carbon number, the alkyl chain length becomes great at a rate of 0.125 nm per one carbon,[104] suggesting that the photoreduction of $MV^{+\cdot}$ is controlled by the electron tunneling probability.

If the electron tunneling prevails, the rate constant for the electron transfer (k) is given by eq. (40)

$$\ln k = -\beta d + \ln k_0 \qquad (40)$$

where d is the distance for electron tunneling and β is a constant. The results shown in Fig. 44 give β of 1.5 nm^{-1}. This value is lower than those reported
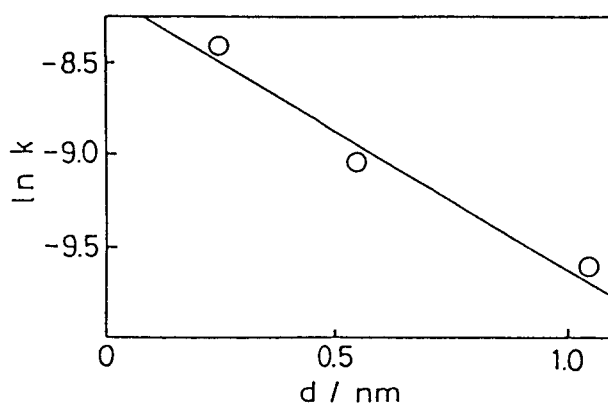

Fig. 44. Dependence of the rate constant of MV^{2+} reduction at the alkanethiol-capped ZnS microcrystals on chain length of capping molecules.

by other investigators[105-107] for electron tunneling through rigid nonconjugated polymers, where β of 8.8 - 12 nm^{-1} were obtained. The β value obtained in this study predicts a barrier height of 0.012 eV for a rectangular barrier,[104] being impracticable for electron tunneling due to its smallness. The result suggest that the capping thiol molecules do not stand vertically on the ZnS particles and/or MV^{2+} penetrates into the capped thiol layer. Small β values of 1.6 - 5 nm^{-1} were reported for photo-induced electron transfer from excited anthracene to Al electrode substrate through a fatty acid monolayer,[108-110] and a β value of the similar magnitude of 1.5 nm^{-1} was reported for electron transfer from a bipyridinium polymer as an electron relay to the redox center of glutathione reductase.[111] To explain the β value of 1.5 nm^{-1}, Willner et al. assumed partial stretching of the polymer chain and a tilt angle between the polymer chain and the electron relay. The same situation would hold in our system, because there is no reason to assume nonflexibility of the modified thiols. Furthermore, there may be free spaces that allow intrusion of MV^{2+} molecules into the capped thiol layers. As described above, the ZnS surfaces are fully capped with alkane thiols, but this does not necessarily mean that there are no unmodified surface sites that allow the intrusion of MV^{2+} molecules into the modified layers. Our estimation of full capping implies that the ZnS surfaces are modified fully from a statical point of view.

Quite different photoreduction behaviors were observed at naked ZnS particles. As shown in Fig. 45, $MV^{+\cdot}$ was produced linearly with illumination time in an initial stage, followed by stagnation. If the initial production rates of $MV^{+\cdot}$ were obtained and plotted against the concentration of MV^{2+}, curve a of Fig. 46 was obtained. The production rate of $MV^{+\cdot}$ was not linearly dependent on the MV^{2+} concentration, which was different from the results of Fig. 43. It has already been reported for photoreduction of MV^{2+} on naked
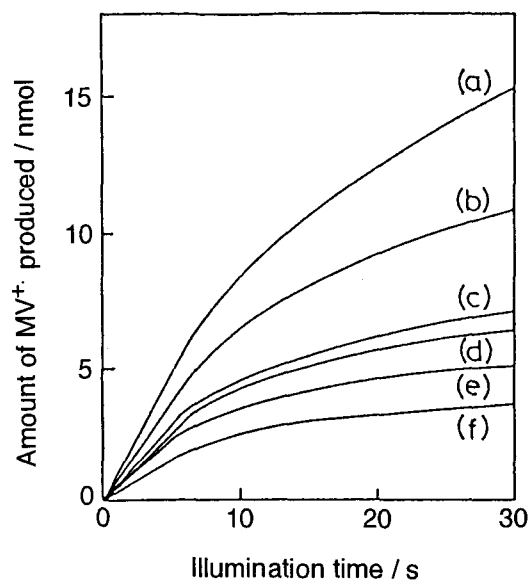
Fig. 45. Time course of MV^+· production for 14 mM bulk ZnS powders. The concentration of MV^{2+}:(a) 1.0 mM, (b) 0.40 mM, (c) 0.30 mM, (d) 0.20 mM, (e) 0.10 mM, (f) 0.05 mM.
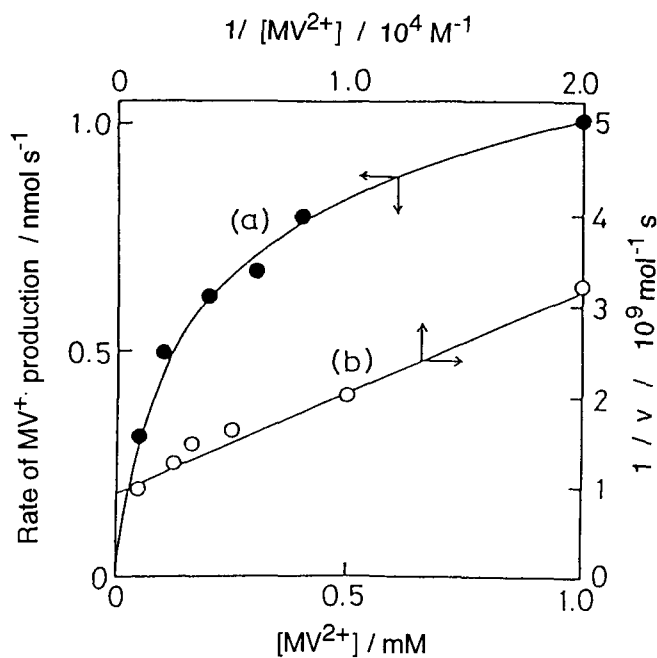

Fig. 46. (a) Rate (v) of MV^+· production obtained at bulk ZnS particles as a function of the concentration of MV^{2+} and (b) Plots of $1/v$ as a function of $1/[MV^{2+}]$.

83

CdS,[112,113] and TiO_2[114] that the photoreduction proceeds via its adsorption on the photocatalyst surfaces. By assuming that adsorption-desorption equilibrium of MV^{2+} on the photocatalyst surfaces is given by eq. (41),

$$k_1(1-\theta)[MV^{2+}] = k_{-1}\theta \qquad (41)$$

and that the production rate (v) of $MV^{+\cdot}$ is linearly proportional to the surface coverage θ, then a Langmuir-Hinshelwood type equation[115,116] prevails in kinetics of photoreduction of MV^{2+}.

$$\frac{1}{v} = \frac{K}{k_2}\left(\frac{1}{[MV^{2+}]}\right) + \frac{1}{k_2} \qquad (42)$$

where k_1 and k_{-1} are the rate constant for the adsorption and desorption, respectively, $K = k_{-1}/k_1$ and k_2 is the rate constant for MV^{2+} reduction. Plots of the results given by curve a of Fig. 46 with use of eq. (42) give curve b of the same figure, evidencing operations of adsorption limited process in the photoreduction of MV^{2+}. The rate constant k_2 obtained from the intercept of the plots is 1.1 nmol s^{-1}.

Considering that the photoreduction of MV^{2+} occurs under adsorption limited process on the naked ZnS, this process may be involved in photoreduction of MV^{2+} in the thiol-capped ZnS if unmodified surfaces were available, being against the experimental results obtained. As already mentioned above, it is believed that the full capping with the thiols was achieved in the present study, which hinders adsorption of MV^{2+} on ZnS surfaces.

4-5 Summary

The size of ZnS microcrystals modified with ethanethiol ,butanethiol and octanethiol was about 4 nm with a narrow size distribution irrespective of the length of alkyl chain. The perfectness of the surface modification by

alkanethiols was confirmed from the evaluation of the number of Zn^{2+} and S^{2-} ions of ZnS microcrystal surfaces using the computer simulation. The rate of photo-induced electron transfer of the capped ZnS microcrystals to MV^{2+} linearly depended on the concentration of MV^{2+} and the evaluated rate constant showed logarithmic dependence on the alkyl chain length of capping reagents, suggesting the electron tunneling was rate-determining. At the bulk ZnS, the photo-induced reduction of MV^{2+} occurred under adsorption limited process with the Langmuir-Hinshelwood mechanism.

Conclusion

This thesis deals with the establishment of photo-induced reaction systems for carbon dioxide fixation. The results and conclusions obtained in this study are summarized as follows.

In chapter 1, photochemical CO_2 fixation in oxoglutarate and pyruvate using ICDH and ME as catalysts was described, which was achieved using CdS and quantized TiO_2 prepared in the interlayer spaces of sodium montmorillonite as semiconductor photocatalysts, MV^{2+} as an electron mediator and either triethanolamine or 2-mercaptoethanol as hole scavengers. Judging from the dependence of the concentration of the substrate and the mediator on the initial production rate of isocitrate and malate, the rate-determining step of photochemical fixation of CO_2 in oxoglutarate and pyruvate was the electron transfer between ICDH and substrate and the electron transfer between $MV^{+\cdot}$ and FNR, respectively. By using selective photooxidation of lactate to pyruvate on CdS, a photochemical conversion system of lactate to malate through pyruvate was established.

In chapter 2, the preparation of quantized ZnS and TiO_2 of different sizes and photocatalytic activities of the prepared semiconductor microcrystals for photoreduction of CO_2 were described. The particle size of the semiconductor microcrystals was controlled by changing the $[Zn^{2+}] / [S^{2-}]$ ratio in the preparation of the ZnS microcrystals and $[Ti(OEt)_4] / [Si(OEt)_4]$ ratio in the preparation of the Q-TiO_2/SiO_2. The prepared ZnS and TiO_2 microcrystals showed activities for photoreduction of CO_2 to formate and in the case of using TiO_2 microcrystal photocatalyst, methane and ethylene also were produced as minor products. The quantum efficiency for the production of these were increased with decreasing the particle size of the ZnS and TiO_2 microcrystals.

In chapter 3, the effect of metal loadings of ZnS microcrystals on photocatalytic activities for CO_2 reduction and photocatalytic activities for CO_2 reduction of ZnS/CdS solid solutions were described. Also described was the effect of charged conditions of stabilizers on photoreduction behaviors of CO_2 on quantized CdS particles. The Cd-loading of ZnS microcrystals was the most effective among the metals examined. The CO_2 photoreduction product by Cd-loaded ZnS microcrystals was formate and the highest quantum efficiency obtained for its production was 32.5%. ZnS/CdS solid solution microcrystals showed low activities for the photoreduction of CO_2. With increasing the mole fraction of CdS the activities for the formate production decreased, while the production of CO was noticed for the mole fraction of CdS of 0.5-0.67. Stabilizers having negative charges such as polyvinylsulfonate and polyacrylic acid gave formate as the reduction products of CO_2, while those having positive charges such as polyethyleneimine and polybrene gave CO. The charged condition of adsorbed stabilizers on the semiconductor photocatalyst may influence the conformation of adsorbed reduction intermediate of CO_2 such as $CO_2^-\cdot$ to give different type of its adsorption such as end-on and side-on adsorption, resulting in different reaction products.

In chapter 4, photoreduction behaviors of MV^{2+} on ZnS microcrystals fully modified with ethanethiol, butanethiol, and octanethiol of about 4 nm diameter with a narrow size distribution and on naked ZnS were described. The rate of photo-induced electron transfer on the alkanethiol-modified ZnS microcrystals showed a linear dependence on the concentration of MV^{2+}, while at bulk ZnS particles the Langmuir-Hinshelwood type kinetics prevailed. It is concluded from the observed logarithmic dependence of the rate constant on the increase of the chain length of the modified alkanethiols that the electron tunneling controls the photo-induced reduction of MV^{2+} on

alkanethiol-modified ZnS microcrystals.

Acknowledgement

References

(1) Taniguchi, I., *Modern Aspects of Electrochemistry*, J. O'M. Bockris, B. E. Conway and R. E. White, Ed.; Plenum Press, **1989**, Vol. 20.

(2) Inoue, T.; Fujishima, A.; Konishi, S.; Honda, K. *Nature* **1979**, 277, 637.

(3) (a) Aurian-Blajeni, B.; Halmann, M.; Manassen, J. *Solar Energy* **1980**, 25, 165.

(b) Halmann, M.; Ulman, M.; Aurian-Blajeni, B. *Solar Energy* **1983**, 31, 429.

(4) Chandrasekaran, K.; Thomas, J. K. *Chem. Phys. Lett.* **1983**, 99, 7.

(5) Halmann, M.; Katzir, V.; Borgarello, E.; Kiwi, J. *Solar Energy Mater.* **1984**, 10, 85.

(6) (a) Willner, I.; Mandler, D. *J. Am. Chem. Soc.* **1989**, 111, 1330.

(b) Goren, Z.; Willner, I.; Nelson, A. J.; Frank, A. J. *J. Phys. Chem.* **1990**, 94, 3784.

(7) Albers, P.; Kiwi, J. *New J. Chem.* **1990**, 14, 135.

(8) Ogura, K.; Kawano, K.; Yano, J.; Sakata, Y. *J. Photochem. Photobiol., A: Chem.* **1991**, 66, 91.

(9) Hirano, H.; Inoue, K.; Yatsu, T. *J. Photochem. Photobiol., A: Chem.* **1992**, 64, 255.

(10) Ishitani, O.; Inoue, C.; Suzuki, Y.; Ibusuki, T. *J. Photochem. Photobiol., A: Chem.* **1993**, 72, 269.

(11) Yamamura, S.; Kojima, H.; Iyoda, J.; Kawai, K. *J. Electroanal. Chem.* **1987**, 225, 287.

(12) Cook, R. L.; MacDuff, R. C.; and Sammells, A. F. *J. Electrochem. Soc.* **1988**, 135, 3069.

(13) (a) Eggins, B. R.; Irvine, J. T. S.; Murphy, E. P.; Grimshaw, J. *J. Chem. Soc., Chem. Commun.* **1988**, 1123.

(b) Eggins, B. R.; Robertson, P. K. J.; Stewart, J. H.; Woods, E. *J. Chem. Soc., Chem. Commun.* **1993**, 349.

(14) Aliwi, S. M.; Al-Jubori, K. F. *Solar Energy Materials* **1989**, 18, 223.

(15) Kanemoto, M.; Ankyu, H.; Wada, Y.; Yanagida, S. *Chem. Lett.* **1992**, 2113.

(16) Junfu, L.; Baozhu, C. Y. *J. Electroanal. Chem.* **1992**, 324, 191.

(17) (a) Henglein, A.; Gutiérrez, M. *Ber. Bunsenges. Phys. Chem.* **1983**, 87 852.

(b) Henglein, A.; Gutiérrez, M.; Fischer, Ch. -H. *Ber. Bunsenges. Phys. Chem.* **1984**, 88, 170.

(18) Tennakone, K.; Jayattissa, A. H.; Punchihewa, S. *J. Photochem. Photobiol., A: Chem.* **1989**, 49, 369.

(19) (a) Hirai, Y.; Aida, T.; Inoue, S. *J. Am. Chem. Soc.* **1989**, 111, 3062.

(b) Inoue, S.; Nukui, M.; Kojima, F. *Chem. Lett.* **1984**, 619.

(c) Komatsu, M.; Aida, T.; Inoue, S. *J. Am. Chem. Soc.* **1991**, 113, 8492.

(20) Craig, C. A.; Spreer, L. O.; Otvos, J. W. *J. Phys. Chem.* **1990**, 94, 7957.

(21) Kitamura, N.; Tazuke, S. *Chem. Lett.* **1983**, 1109.

(22) (a) Kirch, M.; Lehn, J. -M.; Sauvage, J. -P. *Helv. Chim. Acta* **1979**, 62, 1345.

(b) Hawecker, J.; Lehn, J. -M.; Ziessel, R. *J. Chem. Soc., Chem. Commun.* **1983**, 536.

(c) Hawecker, J.; Lehn, J. -M.; Ziessel, R. *J. Chem. Soc., Chem. Commun.* **1985**, 56.

(d) Lehn, J. -M., Ziessel, R. *J. Organomet. Chem.* **1990**, 382, 157.

(23) Calzaferri, G.; Hädener, K.; Li, J. *J. Photochem. Photobiol., A: Chem.* **1992**, 64, 259.

(24) (a) Mandler, D.; Willner, I. *J. Chem. Soc., Perkin Trans. II* **1988**, 997.

(b) Willner, I.; Mandler, D.; Rinkin, A. *J. Chem. Soc., Chem. Commun.* **1986**, 1022.

(25) Tazuke, S.; Kitamura, N. *Nature* **1984**, 309, 148.

(26) (a) Matsuoka, S.; Yamamoto, K.; Pac, C.; Yanagida, S. *Chem. Lett.* **1991**, 2099.

(b) Matsuoka, S.; Kohzuki, T.; Pac, C.; Ishida, A.; Takamatsu, S.; Kusaba, M.; Nakashima, N.; Yanagida, S. *J. Phys. Chem.* **1990**, 94, 2068.

(c) Matsuoka, S.; Yamamoto, K.; Ogata, T.; Kusaba, M.; Nakashima, N.; Fujita, E.; Yanagida, S. *J. Am. Chem. Soc.* **1993**, 115, 601.

(27) Shibata, T.; Kabumoto, A.; Shiragami, T.; Ishitani, O.; Pac, C.; Yanagida, S. *J. Phys. Chem.* **1990**, 94, 2068.

(28) Matsuoka, S.; Kabumoto, A.; Shiragami, T.; Ishitani, O.; Pac, C.; Yanagida, S. *J. Chem. Soc., Chem. Commun.* **1991**, 580.

(29) (a) Sugimura, K.; Kuwabata, S.; Yoneyama, H. *J. Am. Chem. Soc.* **1989**, 111, 2361.

(b) Sugimura, K.; Kuwabata, S.; Yoneyama, H. *Bioelectrochem. Bioenerg.* **1990**, 24, 241.

(30) Brus, L. A. *J. Phys. Chem.* **1986**, 90, 2555.

(31) Zoo, K. Z.; Fendler, J. H. *J. Phys. Chem.* **1991**, 95, 3176.

(32) (a) Yoneyama, H. *Res. Chem. Intermed.* **1991**, 15, 101.

(b) Yoneyama, H. *Critical Reviews in Solid States and Materials Science* **1993**, 18, 69.

(33) (a) Miyoshi, H.; Yoneyama, H. *J. Chem. Soc., Faraday Trans. 1* **1989**, 85, 1873.

(b) Miyoshi, H.; Yamachika, M.; Mori, H.; Yoneyama, H. *J. Chem. Soc., Faraday Trans.* **1990**, 86, 815.

(c) Miyoshi, H.; Tanaka, K.; Uchida, H.; Mori, H.; Sakata, T.; Yoneyama, H. *J. Electroanal. Chem.* **1990**, 295, 71.

(d) Miyoshi, H.; Nippa, S.; Uchida, H.; Mori, H.; Yoneyama, H. *Bull. Chem. Soc. Jpn.* **1990**, 63, 3380.

(34) Bulhoes, L. O.; Zora, A. J. *J. Electroanal. Chem.* **1988**, 248, 159.

(35) Mizen, M. B.; Wrighton, M. S. *J. Electrochem. Soc.* **1989**, 136, 941.

(36) (a) Tanaka, K.; Wakita, R.; Tanaka, T. *J. Am. Chem. Soc.* **1989**, 111, 2428.

(b) Tanaka, K.; Matui, T.; Tanaka, T. *J. Am. Chem. Soc.* **1989**, 111, 3765.

(c) Tanaka, K.; Wakita, R.; Tanaka, T. *Chem. Lett.* **1987**, 1951.

(d) Nagao, H.; Miyamoto, H.; Tanaka, K. *Chem. Lett.* **1991**, 323.

(37) (a) Dérien, S.; Clinet, J-C.; Dunach, E.; Périchon, J. *J. Chem. Soc., Chem. Commun.* **1991**, 549.

(b) Garnier, L.; Pollin, Y.; Périchon, J. *J. Organomet. Chem.* **1989**, 367, 347.

(38) (a) Simpson, T. C.; Durand Jr., R. R. *Electrochim. Acta* **1990**, 35, 1399.

(b) Simpson, T. C.; Durand Jr., R. R. *Electrochim. Acta* **1990**, 35, 1405.

(39) (a) Amatore, C.; Jutand, A. *J. Electroanal. Chem.* **1991**, 306, 141.

(b) (a) Amatore, C.; Jutand, A. *J. Am. Chem. Soc.* **1991**, 113, 2819.

(40) Parkinson, B. A.; Weaver, P. F. *Nature* **1984**, 309, 148.

(41) Ito, Y.; Uozu, Y.; Matsuura, T. *J. Chem. Soc., Chem. Commun.* **1988**, 562.

(42) Akiyama, A.; Bednerski, M.; Kim, M. -J.; Simon, E. S.; Waldmann, H.; Whitesides, G. M. *Chemtech* **1988**, 627.

(43) Siebert, G.; Carsiotis, M.; and Plaut, G. W. E. *J. Biol. Chem.* **1957**,

226, 977.

(44) Ramakrishna, M.; Krishnaswany, N. *Biochem. Biophys. Res. Commun.* **1966**, 25, 378.

(45) (a) Wong, C. H.; Danils, L.; Johnson, W. H. O.; Whitesides,G. M. *J. Am. Chem. Soc.* **1981**, 103, 6227.

(b) Wong, C. H.; Gordon, J.; Cooney, C. L.; Whitesides, G. M. I. *J. Chem. Soc.* **1981**, 46, 4676.

(c) Wong, C. H.; Whitesides, G. M. *J. Am. Chem. Soc.* **1982**, 104, 3542.

(46) Yoneyama, H.; Haga, S.; Yamanaka, S. *J. Phys. Chem.* **1989**, 93, 4833.

(47) Harada, H.; Ueda, T.; Sakata, T. *J. Phys. Chem.* **1989**, 93, 1542.

(48) Mandler, D.; Willner, I. *J. Chem. Soc. Perkin Trans. II* **1986**, 805.

(49) Collman, R. F. *J. Biol. Chem.* **1968**, 243, 2454.

(50) *Enzyme Nomenclature*, Nomenclature Committee of the International Union of Biochemistry, Ed.; Academic Press, **1979**.

(51) *The Chemical Kinetics of Enzyme Action*, Laidler K. J.; Bunting, P. S., Ed., Clarendon Press, **1973**.

(52) Simpananta, P.; Goodridge, A. G. J. Biol. Chem. **1971**, 246, 5754.

(53) Nevaldine, B. H.; Bassel, A. R.; Hsu, R. Y. *Biochim. Biophys. Acta* **1974**, 336, 283.

(54) Cuendet, P.; Grätzel, M. *J. Phys. Chem.* **1987**, 91, 654.

(55) Anpo, A.; Shima, T.; Kodama, S.; Kubokawa, Y. *J. Phys. Chem.* **1987**, 91, 4305.

(56) Al-Thabaiti, S.; Kuntz, R. R. *Langmuir* **1990**, 6, 782.

(57) Fan, F. -R. F.; Leempoel, P.; Bard, A. J. *J. Electrochem. Soc.* **1983**, 130, 1866.

(58) Tomkiewicz, M. *J. Electrochem. Soc.* **1979**, 126, 1505.

(59) Anpo, M.; Chiba, K. *J. Mol. Catal.* **1992**, 74, 207.

(60) Brus, L. E. *J. Phys. Chem.* **1984**, 80, 4403.

(61) Kane, E. O. *Phys. Rev. B* **1978**, 18, 6849.

(62) Vechten, J. A. V. *Phys. Rev.* **1969**, 182, 891.

(63) Ookubo, A.; Kanezaki, E.; Ooi, K. *Langmuir* **1990**, 6, 206.

(64) Grätzel, M., *Modern Aspects of Electrochemistry*, Bockris, J. O'M.; Conway, B. E.; White, R. E., Eds., Plenum Press, **1983**, Vol. 15.

(65) Fox, M. A.; Dulay, M. T. *Chem. Rev.* **1993**, 93, 341.

(66) Sakata, T. *J. Photochem.* **1985**, 29, 205.

(67) Reiche, H.; Bard, A. J. *J. Am. Chem. Soc.* **1979**, 100, 3127.

(68) (a) Kraeutler, B.; Bard, A. J. *J. Am. Chem. Soc.* **1978**, 100, 2239.

(b) Kraeutler, B.; Jaeger, C. D.; Bard, A. J. *J. Am. Chem. Soc.* **1978**, 100, 4903.

(c) Kraeutler, B.; Bard, A. J. *J. Am. Chem. Soc.* **1978**, 100, 5985.

(69) (a) Kakuta, N.; Park, K. H.; Finlayson, M. F.; Ueno, A.; Bard, A. J.; Campion, A.; Fox, M. A.; Webber, S. E.; White, J. M. *J. Phys. Chem.* **1985**, 89, 732.

(b) Ueno, A.; Kakuta, N.; Park, K. H.; Finlayson, M. F.; Bard, A. J.; Campion, A.; Fox, M. A.; Webber, S. E.; White, J. M. *J. Phys. Chem.* **1985**, 89, 3828.

(c) Ueno, A.; Kakuta, N.; Park, K. H.; Finlayson, M. F.; Bard, A. J.; Campion, A.; Fox, M. A.; Webber, S. E.; White, J. M. *J. Phys. Chem.* **1985**, 89, 5028.

(d) Enea, O.; Bard, A. J. *J. Phys. Chem.* **1986**, 90, 301.

(e) Kobayashi, J.; Kitaguchi, K.; Tanaka, H.; Tsuiki, H.; Ueno, A. *J. Chem. Soc., Faraday Trans. 1* **1987**, 83, 1395.

(70) Kanemoto, M.; Shiragami, T.; Pac, C.; Yanagida, S. *J. Phys. Chem.* **1992**, 96, 3521.

(71) Nosaka, Y.; Fox, M. A. *Langmuir* **1987**, 3, 1147.

(72) Katchalsky, A.; Shavit, N.; Eisenberg, H. *J. Polym. Sci.* **1954**, 13, 69.

(73) Weller, H.; Koch, U.; Gutiérrez, M.; Henglein, A. *Ber. Bunsenges. Phys. Chem.* **1984**, 88, 649.

(74) Henglein, A. *Ber. Bunsenges. Phys. Chem.* **1982**, 86, 301.

(75) Henglein, A.; Lilie, J. *J. Phys. Chem.* **1981**, 85, 1246.

(76) Mills, A.; Porter G. *J. Chem. Soc., Faraday Trans. 1* **1982**, 78, 3659.

(77) Furlong, D. N.; Wells, D.; Sasse, W. H. F. *J. Phys. Chem.* **1985**, 89, 1922.

(78) Mau, A. W. -H.; Huang, C. B.; Kakuta, N.; Bard, A. J.; Campion, A.; Fox, M. A.; White, J. M.; Webber, S. E. *J. Am. Chem. Soc.* **1984**, 106, 6357.

(79) Reber, J. -F.; Rusek, M. *J. Phys. Chem.* **1986**, 90, 824.

(80) Eggins, B. R.; McNeil, J. *J. Electroanal. Chem.* **1983**, 148, 17.

(81) Vassiliev, Y. B.; Bagotzky, V. S.; Osetrova, N. V.; Khazova, O. A.; Mayorova, N. A. *J. Electroanal. Chem.* **1985**, 189, 271.

(82) Lippens, P. E.; Lannoo, M. *Phys. Rev. B* **1989**, 39, 10935.

(83) Hashimoto, K.; Fujishima, A. *Annual 59th Meeting of the Chemical Society of Japan*, Abstract vol. I, **1990**, 2200.

(84) Moser, J.; Grätzel, M. *Helv. Chim. Acta* **1982**, 65, 1436.

(85) Chang, An-C.; Pfeiffer, W. F.; Guillaume, B.; Baral, S.; Fendler, J. H. *J. Phys. Chem.* **1990**, 94, 4284.

(86) Moser, J.; Punchihewa, S.; Infelta, P. P.; Grätzel, M. *Langmuir* **1991**, 7, 3012.

(87) (a) Tricot, Y-M.; Porat, Z.; Manassen, J. *J. Phys. Chem.* **1991**, 95, 3242.

(b) Tricot, Y-M.; Manassen, J. *J. Phys. Chem.* **1988**, 92, 5239.

(88) (a) Nosaka, Y.; Fox, M. A. *J. Phys. Chem.* **1986**, 90, 6521.

(b) Nosaka, Y.; Fox, M. A. *J. Phys. Chem.* **1988**, 92, 1893.

(c) Nosaka, Y.; Yamaguchi, K.; Miyama, H.; Hayashi, H. *Chem. Lett.* **1988**, 605.

(d) Nosaka, Y.; Ohta, N.; Miyama, H. *J. Phys. Chem.* **1990**, 94, 3752.

(89) (a) Kamat, P. V.; Dimitrijevic, N. M.; Fessenden, R. W. *J. Phys. Chem.* **1987**, 91, 396.

(b) Gopidas, K. R.; Kamat, P. V. *Langmuir* **1989**, 5, 22.

(90) (a) Steigerwald, M. L.; Alivisatos, A. P.; Gibson, J. M.; Harris, T. D.; Kortan, R.; Muller, A. J.; Thayer, A. M.; Duncan, T. M.; Douglass, D. C.; Brus, L. E. *J. Am. Chem. Soc.* **1988**, 110, 3026.

(b) Bawendi, M. G.; Kortan, A. R.; Steigerwald, M. L.; Brus, L. E. *J. Chem. Phys.* **1989**, 91, 7282.

(c) Kortan, A. R.; Hull, R.; Opila, R. L.; Bawendi, M. G.; Steigerwald, M. L.; Carroll, P. J.; Brus, L. E. *J. Am. Chem. Soc.* **1990**, 112, 1327.

(d) Marcus, M. A.; Flood, W.; Steigerwald, M.; Brus, L. E.; Bawendi, M. *J. Phys. Chem.* **1991**, 95, 1572.

(91) Herron, N.; Wang, Y.; Eckert, H. *J. Am. Chem. Soc.* **1990**, 112, 1322.

(92) (a) Yanagida, S.; Enokida, T.; Shindo, A.; Shiragami, T.; Ogata, T.; Fukumi, T.; Sakaguchi, T.; Mori, H.; Sakata, T. *Chem. Lett.* **1990**, 1773.

(b) Ogata, T.; Hosakawa, H.; Oshiro, T.; Wada, Y.; Sakata, T.; Mori, H.; Yanagida, S. *Chem. Lett.* **1992**, 1665.

(93) (a) Torimoto, T.; Uchida, H.; Sakata, T.; Mori, H.; Yoneyama, H. *J. Am. Chem. Soc.* **1993**, 115, 1874.

(b) Torimoto, T.; Sakata, T.; Mori, H.; Yoneyama, H. *J. Phys. Chem.* **1994**, 98, 3036.

(94) Watanabe, T.; Honda, K. *J. Phys. Chem.* **1982**, 86, 2617.

(95) L. C. Thomas, *Colorimetric Chemical Analytical Methods*, Ed.; Springer-

Verlag, **1980**.

(96) Rossetti, R.; Hull, R.; Gibson, J. M.; Brus, L. E. *J. Chem. Phys.* **1985**, 82, 552.

(97) Wang, Y.; Suna, A.; Mahler, W.; Kosowski, R. *J. Chem. Phys.* **1987**, 87, 7315.

(98) Brus, L. E. *IEEE J. Quantum Electronics* **1986**, 22, 1909.

(99) Weller, H.; Schmidt, H. M.; Koch, U.; Fojtik, A.; Baral, S.; Henglein, A.; Kunach, W.; Weiss, K.; Dieman, E. *Chem. Phys. Lett.* **1986**, 124, 557.

(100) Nosaka, Y. *J. Phys. Chem.* **1991**, 95, 5054.

(101) Nelkowski and Schulz, *Zahlenwerte und Funktionen aus Naturwissenschaft und Technik*, Landolt-Bornstein, Ed.; Springer-Verlag, **1982**.

(102) Widrig, C. A.; Majda, M. *Langmuir*, **1989**, 5, 689.

(103) (a) Ebbesen, T. W.; Levery, G.; Patterson, L. K. *Nature*, **1982**, 298, 545.

(b) Ebbesen, T. W.; Ferraudi, G. *J. Phys. Chem.* **1983**, 87, 3717.

(104) Miller, C.; Cuendet, P.; Grätzel, M. *J. Phys. Chem.* **1991**, 95, 877.

(105) Li, T. T.-T.; Weaver, M. J. *J. Am. Chem. Soc.* **1984**, 106, 6107.

(106) (a) Closs, G. L.; Calcaterra, L. T.; Green, N. J.; Penfield, K. W.; Miller, J. R. *J. Phys. Chem.* **1986**, 90, 3673.

(b) Closs, G. L.; Piotrowiak, P.; MacInnis, J. M.; Fleming, G. R. *J. Am. Chem. Soc.* **1988**, 110, 2652.

(c) Johnson, M. D.; Miller, J. R.; Green, N. S.; Closs, G. L. *J. Phys. Chem.* **1989**, 93, 1173.

(d) Closs, G. L.; Johnson, M. D.; Miller, J. R.; Piotrowiak, P. *J. Am. Chem. Soc.* **1989**, 111, 3751.

(e) Liang, N.; Miller, J. R.; Closs, G. L. *J. Am. Chem. Soc.* **1990**, 112,

5353.

(107) (a) Oevering, H.; Paddon-Row, M. N.; Heppener, M.; Oliver, A. M.; Cotsaris, E.; Verhoeven, J. M.; Hush, N. S. *J. Am. Chem. Soc.* **1987**, 109, 3258.

(b) Paddon-Row, M. N.; Oliver, A. M.; Warman, J. M.; Smit, K. J.; de Haas, M. P.; Oevering, H.; Verhoeven, J. W. *J. Phys. Chem.* **1988**, 92, 6958.

(108) Kuhn, H. J. *J. Photochem.* **1979**, 10, 111.

(109) Killesreiter, H.; Baessler, H. *Chem. Phys. Lett.* **1971**, 11, 411.

(110) Moebius, D. *Ber. Busenges. Phys. Chem.* **1978**, 82 848.

(111) Willner, I.; Lapidot, N.; Riklin, A.; Kasher, R.; Zahvy, E.; Katz, E. *J. Am. Chem. Soc.*, **1994**, 116, 1428.

(112) Henglein, A. *J. Phys. Chem.* **1982**, 86, 2291.

(113) (a) Kuczynski, J. P.; Thomas, J. K. *J. Phys. Chem.* **1983**, 87, 5498.

(b) Kuczynski, J. P.; Milosavljevic, B. H.; Thomas, J. K. *J. Phys. Chem.* **1984**, 88, 980.

(c) Chandrasekaran, K.; Thomas, J. K. *J. Chem. Soc., Faraday Trans. 1* **1984**, 80, 1163.

(114) (a) Duonghong, D.; Ramasden, J.; Grätzel, M. *J. Am. Chem. Soc.* **1982**, 104, 2977.

(b) Moser, J.; Grätzel, M. *J. Am. Chem. Soc.* **1983**, 105, 2977.

(115) Turchi, C. S.; Ollis, D. F. *J. Catal.* **1990**, 122, 178.

(116) Hidaka, H.; Zhao, J.; Pelizzetti, E.; Serpone, N. *J. Phys. Chem.* **1992**, 96, 2226.